Chemical Geology 552 (2020) 119768

Contents lists available at ScienceDirect

Chemical Geology

journal homepage: www.elsevier.com/locate/chemgeo

Extracting Mg isotope signatures of ancient seawater from marine halite: A reconnaissance

Zhiguang Xia[a], Juske Horita[b], Lars Reuning[c,d], Or M. Bialik[e,f], Zhongya Hu[a,g], Nicolas D. Waldmann[e], Chuan Liu[a], Weiqiang Li[a,*]

[a] State Key Laboratory for Mineral Deposits Research, School of Earth Sciences and Engineering, Nanjing University, Nanjing, Jiangsu 210093, PR China
[b] Department of Geosciences, Texas Tech University, TX 79409-1053, USA
[c] Energy and Mineral Resources Group (EMR), Geological Institute, RWTH Aachen University, Wuellnerstraße 2, 52056 Aachen, Germany
[d] Institute for Geosciences, Kiel University, Ludewig-Meyn-Str. 10, 24118 Kiel, Germany
[e] The Dr. Moses Strauss Department of Marine Geosciences, Charney School of Marine Sciences, University of Haifa, Mount Carmel, 31905 Haifa, Israel
[f] Institute of Geology, CEN, University of Hamburg, Bundesstrasse 55, Hamburg 20146, Germany
[g] School of Ocean and Earth Sciences, Tongji University, Shanghai 200092, PR China

ARTICLE INFO

Editor: Oleg Pokrovsky

Keywords:
Halite
Fluid inclusions
Seawater
Magnesium isotopes
Evaporite

ABSTRACT

The Mg/Ca ratio of seawater fluctuated remarkably over the Phanerozoic. The processes that controlled the temporal variation in seawater Mg/Ca ratio may also have caused the secular changes in Mg isotope ratios of seawater. Therefore, the Mg isotope composition of seawater may be useful to understand the long-term variation in seawater chemistry. Different sedimentary carbonates have been proposed as archives of ancient seawater Mg isotope signatures, but each type of carbonate has its limitations. Halite is a common mineral in evaporite deposits and their fluid inclusions may be used to infer the Mg isotope composition of contemporary seawater. In this study, we developed a method to measure the isotope composition of Mg in halite with an accuracy of better than ± 0.1‰ in δ^{26}Mg. The accuracy of the method was verified systematically, using synthetic NaCl solutions, as well as Holocene lacustrine halite samples from the Dead Sea. The δ^{26}Mg values of marine halite samples show a large variation, ranging from −0.1‰ to −1.6‰ relative to the DSM3 international Mg isotope standard. The δ^{26}Mg values of some ancient salt samples are lower than a published model curve for δ^{26}Mg of seawater, and such inconsistency could be explained by 1) isotopic evolution of brines due to mineral precipitation, 2) entrapment of evaporite minerals into halite during halite precipitation or post-depositional deformation, 3) recrystallization and dissolution of pre-existing Mg minerals, and 4) limitations of the model curve of seawater δ^{26}Mg values. Collectively, we suggest that Mg isotopes in halite are a new geochemical proxy to study the secular variations in seawater chemistry, syndepositional and post-depositional processes of evaporite deposits. Our data highlight the importance of understanding the sedimentary background and textural details of evaporites for appropriate interpretations of Mg isotope data from halite.

1. Introduction

The chemical composition of seawater is dynamic and variable over geologic time scale (Korte and Kozur, 2010; Veizer et al., 1999; Veizer et al., 1997). Long-term changes in seawater chemistry have had a profound influence on the form and distribution of marine carbonates (Arvidson et al., 2011; Sandberg, 1983; Stanley and Hardie, 1998), evaporites (Horita et al., 2002; Lowenstein et al., 2001), and life (Fyfe, 1977; Zhuravlev and Wood, 2008). Magnesium and calcium are the major constituents in seawater and seawater Mg/Ca ratios have fluctuated significantly during the Phanerozoic (e.g., Hardie, 1996; Holland, 2005; Lowenstein et al., 2003; Lowenstein et al., 2001; Wikinson and Algeo, 1989), thus reflecting major changes in the global cycling of these two elements (e.g., Edmond et al., 1979; Tipper et al., 2006a; Tipper et al., 2006b; Wikinson and Algeo, 1989). Dolomitization, hydrothermal alteration at mid-ocean ridges, and clay formation on the seafloors have been identified as the key processes that control Mg/Ca ratios in seawater (e.g., Elderfield and Schultz, 1996; Li et al., 2015; Tipper et al., 2006b; Wikinson and Algeo, 1989), and these processes are associated with diverse Mg isotope fractionation behaviors (e.g., Fantle and Higgins, 2014; Higgins and Schrag, 2010; Higgins and Schrag, 2015; Li et al., 2015; Wimpenny et al., 2014). As a

* Corresponding author.
E-mail address: liweiqiang@nju.edu.cn (W. Li).

https://doi.org/10.1016/j.chemgeo.2020.119768
Received 25 November 2019; Received in revised form 16 June 2020; Accepted 24 June 2020
Available online 28 June 2020

consequence, when the Mg/Ca ratio of seawater changed due to the changes in global Mg-Ca cycling, the Mg isotope composition of seawater also likely has changed (Li et al., 2015). Therefore, Mg isotope compositions of seawater may hold clues to understand the global Mg-Ca cycling and the associated geological processes in modern time (De Villiers et al., 2005; Tipper et al., 2006b) and in the geologic past (Bialik et al., 2018; Higgins and Schrag, 2015; Pogge von Strandmann et al., 2014).

Over the last decade, different types of marine carbonates (i.e., calcite, aragonite, and dolomite) have been employed in attempts to reconstruct ancient seawater δ^{26}Mg values, but each of the carbonates has limitations as a seawater δ^{26}Mg archive. Pogge von Strandmann et al. (2014) and Higgins and Schrag (2015) pioneered in using biogenic low-Mg calcite records to reconstruct seawater Mg isotope compositions in the Cenozoic, but considerable inconsistency exists between the two studies in reconstructed seawater δ^{26}Mg. These inconsistencies might result from heterogeneous isotope compositions in limestone, which in turn modulate Mg isotopes in calcite, as these are highly susceptible to post-depositional processes (Hu et al., 2017; Ma et al., 2017). Aragonite has also been used to infer the δ^{26}Mg of seawater, however the instability of aragonite minerals throughout geological timescales limits its applicability to relatively young age samples (Gothmann et al., 2017; Wombacher et al., 2011). By contrast, dolomite is significantly more robust to resist early diagenesis (Li et al., 2019), burial metamorphism processes (Geske et al., 2015; Hu et al., 2017) and hydrothermal alterations (Hu et al., 2019; Perez Fernandez et al., 2017) and may serve as a reliable archive of Mg isotopes. Attempts have been made to use dolomite records to reconstruct ancient seawater δ^{26}Mg values (Li et al., 2015; Li et al., 2019). However, dolomite is commonly viewed as a product of diagenesis, and whether sedimentary dolomite can be used to infer ancient seawater is presently under debate. Some studies emphasized that the isotopic variability of dolomite is due to the evolution of Mg isotopes in pore waters during dolomitization (Blättler et al., 2015; Huang et al., 2015), whereas others suggested that certain massive dolostone units could be "seawater-buffered" (Higgins et al., 2018) that had undergone ample seawater-sediment exchange during early diagenesis, and therefore reaching Mg isotope equilibrium with coeval seawater (Hu et al., 2019; Hu et al., 2017; Li et al., 2019). The development of additional geological archives of seawater δ^{26}Mg is required to address the issues and controversies in carbonate records of seawater Mg isotope signatures.

Halite is one of the most common minerals in evaporite deposits (Warren, 2006). During the evaporation of seawater, precipitation of halite follows immediately after the precipitation of gypsum (Fig. 1), well before precipitation of Mg-bearing evaporite minerals (Bąbel and Schreiber, 2014; McCaffrey et al., 1987; Shalev et al., 2018b). Primary fluid inclusions captured by halite during their crystallization may preserve the physical, chemical, and isotopic signatures of coeval evolved seawater or brine (e.g., Benison et al., 1998; Horita et al., 1991; Horita and Matsuo, 1986; Knauth and Beeuna, 1986; Lowenstein et al., 1998; Roberts and Spencer, 1995). The homogenization temperatures of halite fluid inclusions may represent the paleotemperatures of the evaporative basin (e.g., Benison, 1995; Roberts and Spencer, 1995; Zambito and Benison, 2013). Many studies showed that it is possible to reconstruct the concentrations of Mg^{2+}, Ca^{2+}, and SO_4^{2-} of seawater based on the systematic analysis of primary fluid inclusions from marine halite (e.g., Brennan et al., 2013; Demicco et al., 2005; Holt et al., 2014; Horita et al., 2002; Lowenstein et al., 2001; Spear et al., 2014). Indeed, because of the dramatic difference in valance and ionic radii between Mg^{2+} and Na^{+}, Mg can hardly exist as lattice substitution in halite crystal (Shannon, 1976), thus Mg^{2+} is expected to only occur in fluid and/or mineral inclusions in halite. Therefore, it is possible that fluid inclusions in halite of marine origin may also preserve the primary Mg isotope signals of the seawater.

Multiple techniques have been developed to analyze the chemical composition of individual fluid inclusions, including direct extraction of

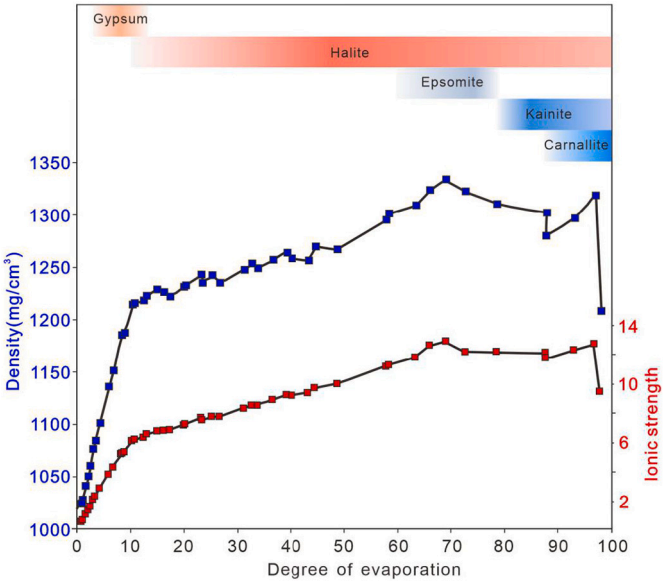

Fig. 1. The precipitation sequence of different evaporite minerals with the Degree of evaporation for modern seawater, based on data by McCaffrey et al. (1987) and Shalev et al. (2018b), and modified from Bąbel and Schreiber (2014). Gypsum-$CaSO_4{\cdot}2H_2O$, Halite-NaCl, Epsomite-$MgSO_4{\cdot}7H_2O$, Kainite-$4KCl{\cdot}4MgSO_4{\cdot}11H_2O$, Carnallite-$KCl{\cdot}MgCl_2{\cdot}6H_2O$.

selected inclusions followed by high sensitivity ion chromatography (IC), inductively coupled plasma mass spectrometry (ICP-MS), or microtitration (Lazar and Holland, 1988; Petrichenko, 1973; von Borstel et al., 2000), and in situ analyses such as laser ablation ICP-MS (Shepherd and Chenery, 1995; Sun et al., 2013), as well as cryo-scanning electron microscopy and environmental SEM that are coupled with micro-beam X-ray spectroscopy (Ayora and Fontarnau, 1990; Spear et al., 2014; Timofeeff et al., 2000). However, the existing methods for chemical analyses of halite inclusions are not applicable to Mg isotopes. The very high Na/Mg mass ratios (> 1000) in bulk halite is a severe challenge to precise and accurate Mg isotope analysis. To date, no study has reported on Mg isotope signatures of fluid inclusions in halite.

In this study, we attempted to explore the possibility of using halite as a geological archive for Mg isotopes in ancient seawater. We developed a method that is capable of effectively separating Mg from extremely high NaCl matrix for Mg isotope analysis of fluid inclusions in halite. The accuracy of the method was validated using synthetic halite solutions and analogue samples from the Dead Sea. With the newly developed method, we measured Mg isotope compositions of selected Phanerozoic marine halite samples, compared the Mg isotope data from marine halite and from other geological records and models, and discussed the factors that could affect the Mg isotope composition of the halite record. Our preliminary data demonstrate the potential of using Mg isotopes signatures in halite to study ancient seawater chemistry, and post-depositional processes the halite experienced.

2. Materials and samples

2.1. Synthetic solution samples

Synthetic solution samples with known Mg concentration and Mg isotope compositions were prepared to mimic the natural halite samples, which have very high Na/Mg ratios (1000–10,000), and thus allow verification of our analytical protocol. The synthetic solution samples were prepared from stock solutions of NaCl and $Mg(NO_3)_2$. The NaCl solution was prepared by dissolving 10 g analytical grade NaCl crystals (Mg concentration: < 0.0108 ppm) in 400 ml of deionized water (18.2 MΩ cm^{-1}); the $Mg(NO_3)_2$ solution was prepared by

Table 1
Recovery of Mg and the measured Mg isotope data for synthetic solution samples.

Exp. no	Na:Mg	Precipitate (μg)	Centrifugate (μg)	Recovery	δ^{26}Mg	2SD	δ^{25}Mg	2SD	n
A-1	2000:1	24.56	2.26	91.6%	−1.02	0.03	−0.53	0.03	2
A-2	2000:1	26.12	1.96	93.0%	−1.00	0.05	−0.52	0.03	2
A-3	2000:1	26.38	2.45	91.5%	−1.01	0.08	−0.54	0.03	2
A-4	2000:1	25.66	1.57	94.2%	−1.00	0.01	−0.54	0.01	2
B-1	2000:1	13.04	0.10	99.3%	−1.02	0.04	−0.51	0.05	2
B-2	2000:1	27.95	0.29	99.0%	−1.02	0.04	−0.53	0.03	2
B-3	2000:1	47.01	4.59	91.1%	−1.01	0.04	−0.53	0.00	2
C-1	4000:1	13.56	5.02	73.0%	−1.02	0.01	−0.52	0.01	2
C-2	1000:1	22.60	1.52	93.7%	−1.05	0.02	−0.53	0.02	2
C-3	500:1	24.66	0.71	97.2%	−1.04	0.07	−0.55	0.03	2
HPS932001	10,000:1	8.88	0.43	95.3%	−2.93	0.08	−1.50	0.05	2
$Mg(NO_3)_2$		–	–	–	−0.98	0.04	−0.50	0.01	2

dissolving 0.124 g analytical grade $Mg(OH)_2$ in 50 ml of 2% HNO_3.

Synthetic solution samples of different Na/Mg ratios were prepared from the stock solutions. Different amounts of the $Mg(NO_3)_2$ solution (either a stock solution prepared from the dissolution of $Mg(OH)_2$ solid or a single element standard solution from High Purity Standards) were mixed with 10 ml of the prepared NaCl solution within a pre-cleaned 15 ml centrifuge tube for each synthetic solution sample. Four groups of synthetic solution samples were prepared: Group A samples (n = 4) contained about 30 μg Mg with a Na/Mg ratio of 2000; group B samples (n = 3) have a constant Na/Mg ratio of 2000, but variable amount of Mg (from 15 to 50 μg); group C samples (n = 3) have a constant amount of Mg (25 μg), but variable Na/Mg ratios, from 4000:1 for C-1, to 1000:1 for C-2, and 500:1 for C-3. Additionally; a group D sample with a Na/Mg ratio of 10,000 was made, using a Mg isotopic standard solution (HPS932001). The details of the synthetic solution samples are listed in Table 1.

2.2. Natural halite samples

Natural halite samples were collected from evaporite deposits ranging in ages from the Cambrian to the Holocene (Table 2). Most of these samples have been well characterized in literature, including their locations, geologic settings, and stratigraphic information (e.g., Belmaker et al., 2013; Biehl et al., 2014; Fanlo and Ayora, 1998; Holser et al., 1984; Horita et al., 1991; Horita et al., 1996; Horita et al., 2002; Kampschulte et al., 1998; Kovalevych et al., 2002; Sirota et al., 2016; Zak, 1967; Zak, 1997). Details about the DSDP samples are available in DSDP reports and publications (http://deepseadrilling.org/i_reports.htm; Hinz and Winterer, 1984; Ryan et al., 1973). Most of the samples analyzed in this study have been screened by experts in previous studies of reconstructing the chemical composition of ancient seawater.

In general, except for the Holocene halite samples from the Dead Sea, which were formed in a lacustrine environment, all other halite samples were of marine origin. Detailed fluid inclusion studies on the same halite samples from literature show that some of the halite samples were precipitated from brines that had reached the K-Mg salt saturation stage (IZ-2, DSDP546, Kepuer-4, CAR12-2 & 12-3, Siberia-2), and halite in some samples (TWR-480 & 515 and WIPP-2) may have co-precipitated with polyhalite ($K_2SO_4{\cdot}MgSO_4{\cdot}2CaSO_4{\cdot}2H_2O$).

2.2.1. Cenozoic

Holocene lacustrine halite deposits were taken from an outcrop in Ein Gedi, Israel, several meters above the Dead Sea level in 2018. A total of seven halite samples were collected from an evaporite sequence interbedded by fine detrital layers (Fig. 2). The halite samples are relatively loose, composed of millimeter to sub-millimeter halite crystals. These samples were taken for the purpose of method validation.

Sample IZ-2 was taken from the Plio-Pleistocene (1 to 2 Ma) Sedom Formation in the Dead Sea valley in Israel. The Sedom Formation consists mainly of halite, cyclically interbedded with gypsum, anhydrite, dolomite and minor amounts of silt, marl and clay (Stein et al., 2000). Previous fluid inclusion analysis indicated that brine entrapped within the sample appeared to be saturated with sylvite, the brine in the inclusion of one sample has been found to be saturated with carnallite. Chemical composition data suggests that the brine in this basin was 20–30% depleted in Mg and SO_4^{2-} relative to modern seawater (Horita et al., 2002).

Sample DSDP-134 is Upper Miocene in age, it was collected from a DSDP drill core (Ryan et al., 1973) that was aimed to recover the evaporite sequence produced during the Messinian Salinity Crisis (~5.96–5.33 Ma) of the Mediterranean, when it is estimated that there are between 821 ± 50 and 927 ± 50 thousand km^3 of evaporites were deposited (Bąbel and Schreiber, 2014; Haq et al., 2019; Meilijson et al., 2019). Dolomitization is widely developed in the Mediterranean during this period (de Lange and Krijgsman, 2010; Lu and Meyers, 1998; Vengosh et al., 1994).

2.2.2. Mesozoic

Sample DSDP-546 is also from a DSDP drill core (Clement and Holser, 1988) which recovered early Jurassic evaporite sequences in offshore Morocco. The evaporite deposits are mainly composed of halite and gypsum/anhydrite, but also contain significant amounts of potash salts (Clement and Holser, 1988). The brine in the fluid inclusion in the halite was also found to be close to the saturation point of carnallite (Horita et al., 2002).

Four halite samples from the Triassic were analyzed in this study. Sample Keuper-4 was taken from a Late Triassic evaporite sequence in France, in which polyhalite is reported to be present along grain boundaries of halite (Fanlo and Ayora, 1998). Fluid inclusion data suggest that the evaporite formed from a highly evaporated brine and the brine in the inclusions in the halite sample appeared to be saturated with sylvite and carnallite (Horita et al., 2002). The other three Triassic samples are from the Netherlands Röt Formation (age: 251.2–247.2 Ma; sample ID; TWR-480 & 515) that were taken from layers showing chevron crystals in halite. Chevron crystals reach 2 cm in length and typically have milky cores and a clear rim. The milky halite shows an internal growth zonation outlined by cubic one-phase fluid inclusions typically ranging in size of 1 to 100 μm. The brine in the fluid inclusions of these salts are interpreted to be trapped during the middle stage of brine evaporation, but polyhalite occurs as inclusions along grain boundaries (Kovalevych et al., 2002).

Polyhalite was widely developed during the Triassic period in Sichuan Basin of China (e.g., Gong et al., 2018; Wang and Zheng, 2014; Zhong et al., 2018), and three polyhalite samples (sample ID: ZK601-18 & 21 & 23) from boreholes were analyzed for this study. These polyhalites are mainly tabular and granular texture, and mostly form a banded structure with gypsum (Zhong et al., 2018).

2.2.3. Paleozoic

Three halite samples analyzed in this study are Permian in age.

Table 2
Elemental concentrations and Mg isotope compositions of natural halite samples analyzed in this study.

Exp. no	Sample weight (g)	Location	Formation/group	Stratigraphic age	Na (ppm)	Mg (ppm)	Ca (ppm)	Na/Mg (mass ratio)	Ca/Mg (mass ratio)	δ^{26}Mg	2SD	δ^{25}Mg	2SD	n
10-25-1	1.908	Israel	Ze'elim Fm.	Holocene	59,746	62.9	48	950	0.8	−0.63	0.03	−0.34	0.05	2
10-25-2	1.474	Israel	Ze'elim Fm.	Holocene	47,176	207.8	123	227	0.6	−0.63	0.01	−0.33	0.01	2
10-25-2.5	1.482	Israel	Ze'elim Fm.	Holocene	44,114	362.5	278	121	0.8	−0.59	0.01	−0.31	0.04	2
10-25-3	1.599	Israel	Ze'elim Fm.	Holocene	45,960	298.4	214	154	0.7	−0.61	0.05	−0.31	0.04	2
10-25-4	1.675	Israel	Ze'elim Fm.	Holocene	49,336	344.0	221	143	0.6	−0.58	0.05	−0.30	0.02	2
10-25-5	1.511	Israel	Ze'elim Fm.	Holocene	44,855	441.1	316	101	0.7	−0.57	0.04	−0.29	0.06	2
10-25-6	1.885	Israel	Ze'elim Fm.	Holocene	56,442	235.6	303	239	1.3	−0.58	0.02	−0.31	0.04	2
IZ-2-(1)	0.641	Israel	Sedom FM	Plio-Pleistocene	20,537	24.8	79	829	3.2	−0.90	0.10	−0.46	0.09	2
IZ-2-(2)	0.726	Israel	Sedom FM	Plio-Pleistocene	23,433	24.0	56	975	2.3	−0.84	0.08	−0.41	0.03	2
DSDP134	1.135	Mediterranean	DSDP Site 134/Core-10/Sec2	Miocene	37,279	34.3	412	1088	12.0	−0.41	0.02	−0.19	0.02	4
DSDP546-1	0.755	Offshore Morocco	DSDP Site 546/18-6/92-97	Early Jurassic	23,183	7.7	147	3010	19.1	−0.18	0.01	−0.08	0.00	2
DSDP546-2	0.759	Offshore Morocco	DSDP Site 546/18-6/92-97	Early Jurassic	23,757	8.0	45	2969	5.7	−0.09	0.03	−0.04	0.01	2
Keuper-4-1	0.961	France	Keuper	Late Triassic	30,767	3.0	48	10,255	16.1	−1.05	0.02	−0.52	0.03	2
Keuper-4-2	0.975	France	Keuper	Late Triassic	31,220	3.1	51	10,071	16.5	−1.01	0.09	−0.54	0.00	2
T-480.01	1.350	Netherlands	Röt FM	Early Middle Triassic	43,355	18.0	836	2411	46.5	−0.44	0.03	−0.22	0.00	2
T-480.04	1.646	Netherlands	Röt FM	Early Middle Triassic	52,264	6.9	94	7538	13.6	−0.53	0.07	−0.28	0.02	4
T-515	1.744	Netherlands	Röt FM	Early Middle Triassic	55,493	6.0	25	9313	4.2	−0.50	0.03	−0.26	0.05	3
Z2-2	1.705	Netherlands	Zechstein 2 FM	Late Permian	54,647	110.0	393	497	3.6	−1.24	0.00	−0.62	0.05	2
Z2-7	1.615	Netherlands	Zechstein 2 FM	Late Permian	51,555	34.1	203	1510	5.9	−1.25	0.03	−0.62	0.00	2
WIPP-2-1-(1)	1.039	New Mexico (U.S.A.)	Salado	Late Permian	33,654	4.0	363	8326	89.8	−1.57	0.04	−0.78	0.00	2
WIPP-2-1-(2)	1.883	New Mexico (U.S.A.)	Salado	Late Permian	53,013	6.0	518	8835	86.4	−1.66	0.05	−0.84	0.04	2
WIPP-2-2	1.220	New Mexico (U.S.A.)	Salado	Late Permian	36,560	4.3	410	8502	95.4	−1.35	0.10	−0.70	0.02	2
AW86-46-1	0.826	Western Canada	Prairie	Middle Devonian	24,963	4.9	976	5129	200.5	−0.63	0.06	−0.31	0.03	2
AW86-46-2	1.135	Western Canada	Prairie	Middle Devonian	32,463	5.6	1671	5814	299.3	−0.55	0.04	−0.29	0.04	2
CAR12-2-1	1.822	Western Australia	Carribuddy	Lower Silurian	55,947	0.6	6	94,825	10.0	−0.96	0.07	−0.49	0.05	2
CAR12-3-1	1.656	Western Australia	Carribuddy	Lower Silurian	51,080	9.4	255	5434	27.1	−0.90	0.01	−0.45	0.03	2
CAR12-3-2	1.245	Western Australia	Carribuddy	Lower Silurian	37,500	7.0	210	5357	30.0	−0.82	0.08	−0.42	0.06	2
Siberia-2	1.727	East Siberia	Angarskaja/Usolskaja	Lower Cambrian	52,193	0.8	47	65,241	58.2	−0.91	0.11	−0.44	0.12	3
ZK601-18	Triassic polyhalite from southwest China									−0.96	0.05	−0.49	0.02	2
ZK601-21	Triassic polyhalite from southwest China									−0.95	0.05	−0.50	0.05	2
ZK601-23	Triassic polyhalite from southwest China									−1.03	0.04	−0.53	0.02	2
HPS932001	Na/Mg = 5000:1									−2.93	0.01	−1.51	0.01	2
HPS932001	Na/Mg = 2000:1									−2.86	0.05	−1.46	0.01	2
HPS932001	Na/Mg = 1000:1									−2.97	0.04	−1.51	0.07	2
HPS909104	Na/Mg = 5000:1									−0.68	0.04	−0.33	0.06	2
HPS909104	Na/Mg = 5000:1, Ca/Mg = 50:1									−0.68	0.05	−0.35	0.01	2

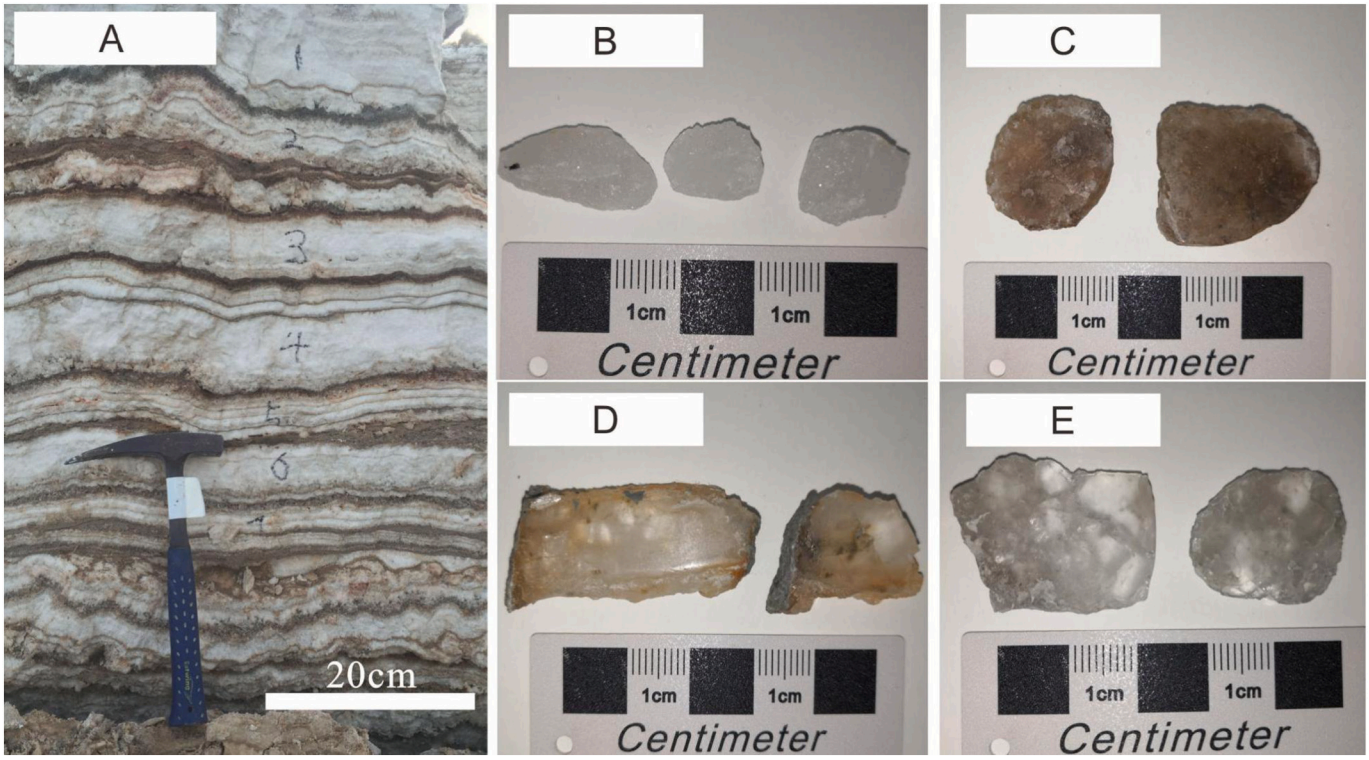

Fig. 2. A) Field outcrop photograph of altering layers of halite with detritus (Holocene, Dead Sea); B to E) Hand specimens photographs of halite samples from Mediterranean, offshore Morocco, France and New Mexico (U.S.A.).

Sample WIPP-2 is from the lower unit of the Late Permian Salado Formation that consists primarily of thick halite beds with minor interbedded anhydrite, polyhalite and clastics. The bedded halite contains abundant primary, chevron inclusions (Horita et al., 1991). Sample WIPP-2 is interpreted to be deposited at the early stage of halite precipitation far before the precipitation of K-/Mg-bearing salts (Horita et al., 1991). The other two samples (sample ID: Z2, Z7) are from the Zechstein 2 Formation (age: 259–254 Ma), which consists of coarse to very coarse crystalline, massive halite interbedded with thin polyhalite beds and some potassium-magnesium salt (kieserite, carnallite and sylvite) layers near the top. Some grains show sub-grain boundaries. No primary growth zonation is observed in the halite crystals. The fluid inclusions in the two Zechstein samples have a relatively low abundance, they generally occur at the grain boundaries and have a typical circular shape. These characteristics indicate that the two samples experienced significant recrystallization (Biehl et al., 2014; Kovalevych et al., 2002).

Sample AW86-46 is from the Middle Devonian Prairie Formation, which consists of halite with thin interbeds of anhydrite, with a sylvite layer at the top of the Prairie formation. The sample analyzed in this study is interpreted to have formed in the early to middle stages of halite precipitation (Horita et al., 1996).

Two samples (CAR12-2 & 12-3) are taken from the Lower Silurian Carribuddy Group, which consists of bedded halite and anhydrite (Cathro et al., 1992). Fluid inclusion analyses suggest that the two samples were precipitated from a brine that was saturated with carnallite (Horita et al., 2002).

The oldest halite sample (Siberia-2) analyzed in this study is from the Early Cambrian, the halite was interpreted to be precipitated from a brine at the carnallite saturation stage (Horita et al., 2002).

3. Experimental methods

3.1. Chemical analyses

Before sampling, the surface of each halite sample was cleaned by wiping with lint-free laboratory paper towels (Kimwipes®), then 1–2 g of halite was scraped off the rock salt using a tungsten carbide scraper. The sample was subsequently dissolved in 12 ml deionized water. A 100 μl fraction of the supernatant of the dissolved salt was extracted and diluted to 2 ml in 2% double-distilled HNO_3. The elemental concentrations of Mg, Ca, and Na were measured, using an inductively coupled plasma optical emission spectrometer (ICP-OES, Skyray ICP-3000) at the State Key Laboratory for Mineral Deposits Research, Nanjing University. A series of gravimetrically prepared multi-element standards were used as the calibrating standards for the ICP-OES analysis, and the uncertainty of the elemental analysis was within ± 10% (2RSD, or two times of relative standard deviation).

3.2. Isotopic analyses

3.2.1. Purification of Mg

Based on the measured Mg concentrations for each dissolved sample, an aliquot of dissolved salt solutions that contained > 10 μg Mg was taken for Mg isotope analysis. Magnesium was firstly purified using the precipitation technique, taking advantage of the low solubility of $Mg(OH)_2$ ($Ksp_{Mg(OH)2} = 1.9 \times 10^{-13}$, T = 298.15 K, Dean, 1990). 3 ml of a 1 mol/l NaOH solution was added to a dissolved halite solution to increase the solution pH and form $Mg(OH)_2$. It should be noted that at a low concentration, $Mg(OH)_2$ occurs in a gel form in aqueous solutions that would not settle. To promote precipitation of $Mg(OH)_2$, 1 day after the addition of NaOH, about 30 μL 23.3 mmol/l $FeCl_3$ solution was added to the solution to form $Fe(OH)_3$ that coagulated with $Mg(OH)_2$, which can then be recovered as a solid and separated from the aqueous solution by centrifuging. The centrifugation was performed several hours after the addition of $FeCl_3$ at 5000 rpm for 15 min. For each

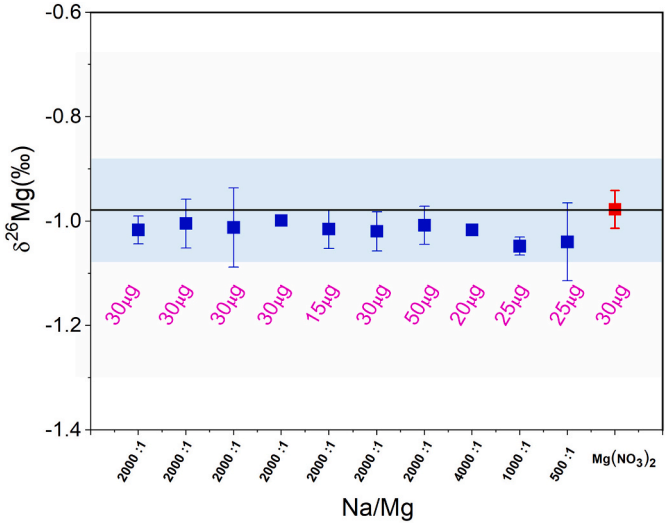

Fig. 3. Test of Mg isotope analytical method based on synthetic solution samples. The red square represents the Mg isotope composition of pure $Mg(NO_3)_2$, and the blue squares represent the measured Mg isotope data for synthetic solution samples after purification. The mass of Mg in each sample is noted in magenta. (For interpretation of the references to color in this figure legend, the reader is referred to the web version of this article.)

sample, the recovery of Mg was determined by measuring the mass of Mg in the precipitate and supernatant, using ICP-OES.

The above precipitation method efficiently separates Mg from Na, the dominant matrix element, but the precipitated Mg was contaminated with Fe and Ca that also form hydroxides. The precipitated hydroxides were separated by centrifugation, gently rinsed with deionized water, and finally dissolved in HCl. Further purification of Mg was achieved using conventional ion-exchange chromatography. Firstly the dissolved sample was treated using anion exchange chromatography that was designed for iron isotope analysis (Du et al., 2017). The sample is dissolved in 0.1 ml 7 M HCl, loaded onto a custom-made Teflon micro-column that contained 0.2 ml Bio-Rad AG MP-1 resin, then eluted by 7 M HCl in 0.5 ml increments. But instead of collecting Fe, we collected the eluent that contained Mg and Ca. The collected eluent was evaporated to dryness and then was treated with 0.5 ml concentrated nitric acid and evaporated on the hotplate at 95 °C. This procedure was repeated three times to convert salts to nitrate form for cation exchange chromatography.

The cation exchange column chemistry followed an established two-stage ion exchange procedure for Mg purification (Hu et al., 2017). The first stage ion exchange procedure is the same as the one used for the K isotope (Li et al., 2016), and is used to remove Ca, Na, Al and other cations. The sample was dissolved in 0.5 ml 1.5 N HNO_3 and loaded onto a quartz glass column that contained 1 ml Biorad cation exchange resin AG50W-X12 (100–200 mesh), Mg is collected after using 1.5 N HNO_3 to remove Na. To ensure complete removal of Ca and Na, the procedure was repeated up to three times for high Ca content samples. For the second stage column chemistry, the samples were dissolved in 0.5 ml mixed acid (0.2 N HNO_3 + 0.05 N HF) and loaded onto a custom-made Teflon column that contained 0.2 ml Biorad AG50W-X8 (100–200 mesh) cation exchange resin. The resin was successively eluted using the mixed acid (0.2 N HNO_3 + 0.05 N HF), 0.5 N HNO_3, 1 N HNO_3, and Mg is collected with 1.5 N HNO_3.

After the above ion-exchange column treatments, the total matrix elements accounted for < 1% of Mg, and the recovery for Mg during ion-exchange chromatography was > 95%. The recovery of 95% is sufficient to avoid measurable artificial Mg isotope fractionation during column chemistry. The total procedural blank is < 30 ng for Mg, which is < 0.3% of the total Mg in each sample and therefore considered negligible.

3.2.2. Magnesium isotope analysis

Magnesium isotope compositions were measured with a Thermo Scientific NEPTUNE Plus multi-collector mass spectrometer (MC-ICP-MS) at the State Key Laboratory for Mineral Deposits Research, Nanjing University, China. The instrument operates on a standard low resolution, wet plasma mode, with a solution uptake rate of 100 μL/min. A standard-sample-standard bracketing analytical routine was used for correction of the instrumental mass bias. A pure in-house Mg solution from High Purity Standards Company (Lot No. HPS909104) was used as the bracketing standard for Mg isotope analysis. The sample concentration generally matched the in-house standard to better than 10%. A 40 s on-peak acid blank was measured before each analysis. Each Mg isotope ratio measurement consisted of fifty 4-s integrations, and the typical internal precision (2 standard error or 2SE) was better than ± 0.04‰ for $^{26}Mg/^{24}Mg$ and ± 0.02‰ for $^{25}Mg/^{24}Mg$. Analytical accuracy was assessed by the analysis of international Mg isotope standards DSM3 and Cambridge1, USGS igneous rock standards, seawater, as well as synthetic solution samples, which were treated as unknown samples and analyzed.

Magnesium isotope data were reported relative to the international Mg isotope standard (DSM3), using conventional δ notation to express per thousand deviations from DSM3: $\delta^{2x}Mg = (^{2x}Mg/^{24}Mg_{sample} - {}^{2x}Mg/^{24}Mg_{DSM3}) / (^{2x}Mg/^{24}Mg_{DSM3}) \times 1000$, where x = 5 or 6.

The $\delta^{26}Mg$ value of the pure Mg solution HPS909104 relative to international standard DSM3 has been well characterized, using three different types of MC-ICP-MS at the University of Wisconsin-Madison and Nanjing University for nearly 10 years ($\delta^{26}Mg$ = 0.66‰ relative to DSM3, Li et al., 2011, 2012, 2019). The measured $\delta^{26}Mg$ values of the seawater and rock standards matched the published values in the literature within ± 0.10‰, and mostly within ± 0.05‰.

4. Results

4.1. Synthetic solution samples

The recovery of Mg in the synthetic solution samples were all above 90%, except for C-1 (Table 1). The $\delta^{26}Mg$ values of Mg in A, B, and C group samples after purification were between −1.05‰ and − 1.00‰, with an average of −1.02 ± 0.03‰ (2SD, n = 20; Table 1, Fig. 3). For comparison, the initial pure $Mg(NO_3)_2$ solution has a $\delta^{26}Mg$ of −0.98 ± 0.04‰ (2SD, n = 2). Group D samples have the highest Na/Mg ratio (10,000:1), and the measured $\delta^{26}Mg$ values are −2.93 ± 0.08‰ (2SD, n = 2), which is also consistent with the $\delta^{26}Mg$ of the original pure Mg solution ($\delta^{26}Mg$ = −2.90 ± 0.13‰ 2SD, n = 48 Li et al., 2012). Therefore, our tests of the synthetic solution samples demonstrated the accuracy of the analytical method for Mg isotopes.

In addition, the in-house Mg standards (HPS932001 and HPS019104) processed the same way as the sample (including the precipitation stage). The $\delta^{26}Mg$ values of HPS932001 range from −2.85 to −2.98‰ and the HPS909104 are −0.66 to −0.70‰, which is consistent with the previous studies from the laboratory of Wisconsin-Madison and Nanjing University (HPS909104: $\delta^{26}Mg$ = −0.66‰ relative to DSM3; HPS932001: $\delta^{26}Mg$ = −2.93‰ relative to DSM3, Li et al., 2011, 2012, 2019).

4.2. Natural halite samples

4.2.1. Chemical compositions of halite

The concentrations of the major elements in the halite samples are shown in Table 2. The Na/Mg mass ratio of the halite samples vary remarkably, from 1.0×10^2 to 9.5×10^4, and the Ca/Mg mass ratio ranged from 0.6 to 299.3. Compared with ancient halite samples, the

Ca/Mg and Na/Mg ratios of the Holocene halite samples are relatively low. The high Na contents in the dissolved halite solution and thus high Na/Mg ratios are expected. Some samples have high calcium contents, which may be caused by the dissolution of anhydrite minerals. Since Mg content in anhydrite is very low (Kushnir, 1982; Lu et al., 2002), the Mg introduced by partial anhydrite dissolution is negligible.

4.2.2. Magnesium isotope compositions

The Holocene lacustrine halite samples from the Dead Sea have very uniform δ^{26}Mg values with an average of −0.60 ± 0.05‰ (2SD, n = 14). For comparison, modern Dead Sea brine has δ^{26}Mg of −0.58‰ (Shalev et al., 2018a). A considerable variation in the δ^{26}Mg values exists among the ancient halite samples of different ages (Table 2).

The δ^{26}Mg values of the Plio-Pleistocene Sedom Formation halite range from −0.90 to −0.84‰ (IZ-2), but a Miocene Mediterranean halite sample has a δ^{26}Mg of −0.41‰ (DSDP134). The δ^{26}Mg values of Early Jurassic offshore Morocco halite between −0.09 and −0.18‰ (DSDP546). The δ^{26}Mg of a halite sample from the Late Triassic Keuper formation range from −1.05 to −1.01‰ (Keuper-4). The halite from the Late Permian Salado Formation has a relatively more negative δ^{26}Mg value of −1.35 to −1.66‰ (WIPP-2). The δ^{26}Mg values of a halite sample from the Middle Devonian Prairie Formation are −0.63 to −0.55‰ (AW86-46) and δ^{26}Mg values of −0.82‰ to −0.96‰ (CAR12–2 & 12–3) are measured for halite samples from the Lower Silurian Carribuddy Group. The halite sample from the Lower Cambrian has δ^{26}Mg of −0.91‰ (Siberia-2).

Additionally, the Mg isotopes of five halite samples from the Netherlands have been measured, the recrystallized halite samples (Z2-2 and Z2-7) of Lopingian (Permian) age have δ^{26}Mg value around −1.25‰, whereas the pristine halite samples of Anisian (Triassic) age that do not show any recrystallization texture (TWR-480 & 515) have δ^{26}Mg around −0.50‰. Three Triassic polyhalite samples (ZK601-18 & 21 & 23) from the Sichuan basin in southwest China show uniform Mg isotopic compositions, with δ^{26}Mg value around −1.00‰.

5. Discussion

5.1. Validity of Mg isotope analysis for halite

In our experiments, Mg was precipitated as $Mg(OH)_2$ form by increasing the pH of the solution using NaOH. The Mg isotope fractionation factors between brucite and solution had been experimentally calibrated by Li et al. (2014), who reported a $\Delta^{26}Mg_{brucite\text{-}solution}$ fractionation of −0.2‰ at 22 °C. This fractionation factor is used in a Rayleigh fractionation model to simulate the process that precipitates Mg in the form of $Mg(OH)_2$, and the results together with experimental results are shown in Fig. 4. Modeling results show that due to the small fractionation factor between brucite and solution, even when the recovery is as low as 70%, the inaccuracy caused by incomplete $Mg(OH)_2$ precipitation for the measured δ^{26}Mg is still within the long-term external precision (± 0.1‰) for Mg isotope analysis. It should be noted that in our study, the recovery for the majority of samples were above 90% (Table 1; Fig. 4). Furthermore, the measured Mg isotope data for synthetic solution samples with different Na/Mg ratios match those of the pure, original $Mg(NO_3)_2$ solutions (Table 1) well within external analytical error (Table 1; Fig. 4). Both experiments and modeling results, therefore, demonstrate that the experimental method developed in this study is suitable for the analysis of Mg isotopes in natural halite to an accuracy of ± 0.1‰ in δ^{26}Mg.

The validity of the analytical method is further supported by a case study of the Holocene halite. As shown in Fig. 5, the Mg isotope compositions of those halite samples (around −0.60‰) are consistent with the Mg isotope composition of the modern Dead Sea brine (δ^{26}Mg = −0.58‰) reported by Shalev et al. (2018a). The Mg isotope signatures of the salts do not show variations along with the vertical depositional profile over 50 cm, despite the distinct layering between white pure halite and dark halite horizons that contain clays. More importantly, the results demonstrate a lack of Mg isotope fractionation between Mg trapped within fluid inclusions in halite crystals or in interstitial fluids and the Mg in brine, from which the halite is precipitated. Therefore, modern halite can record the Mg isotope signatures of the corresponding coeval brines. Therefore, if no Mg isotope fractionation occurs during post-depositional processes, it is theoretically viable to evaluate the Mg isotope composition of ancient brines by analyzing ancient marine halite.

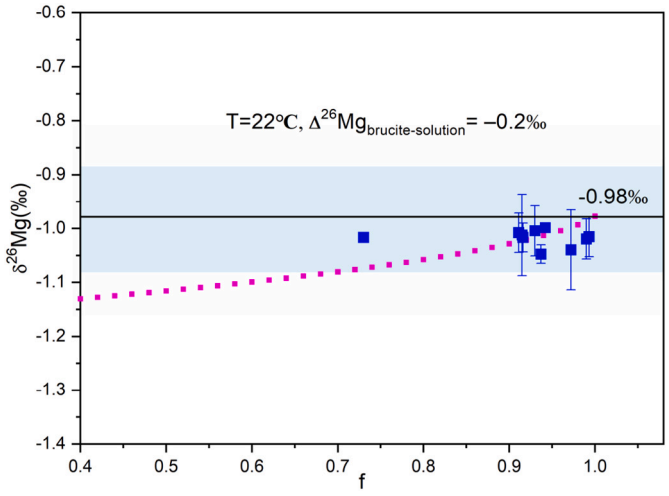

Fig. 4. The plot of measured δ^{26}Mg values versus recovery for synthetic solution samples. The blue squares represents the measured Mg isotope values of synthetic solution samples, and the dotted line represent the trend of expected Mg isotope data for $Mg(OH)_2$ precipitates at different recovery, calculated using a Rayleigh fractionation model. Error bars denote 2 standard deviations of Mg isotope data for each sample. The horizontal line and the shaded area represent the Mg isotope composition of the initial $Mg(NO_3)_2$ solution and the external uncertainty of Mg isotope analysis, respectively. (For interpretation of the references to color in this figure legend, the reader is referred to the web version of this article.)

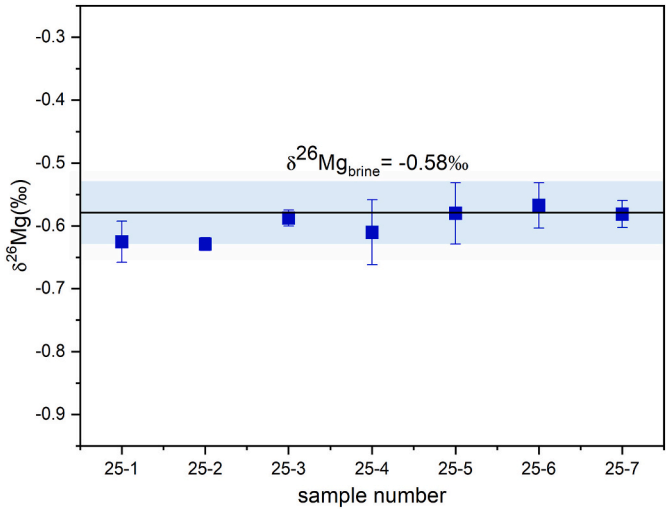

Fig. 5. Comparison of the Mg isotope composition of Holocene halite (blue square) and the brine (horizontal line) from the Dead Sea. The blue squares represent the Mg isotope values of the halite. Error bars denote 2 standard deviations of Mg isotope data for each sample. The shaded area represents the uncertainty of δ^{26}Mg of Dead Sea brine, as reported by Shalev et al. (2018a). (For interpretation of the references to color in this figure legend, the reader is referred to the web version of this article.)

Another fundamental question regarding the method in this study is its reproducibility for analysis of halite from evaporite deposits. Indeed, a bulk halite dissolution method has to be used to collect enough Mg for precise isotope analysis, yet it is possible that secondary fluid inclusions or mineral inclusions are sampled together with the primary fluid inclusions for Mg isotope analysis. One way to assess this issue is to perform parallel analyses on different parts of a halite sample to check the homogeneity of the isotopic signal at cm scale. If a halite sample contains Mg of different origins with spatial heterogeneity (e.g., secondary fluid inclusions trapped in sealed fractures and Mg-bearing evaporite minerals), then the sample likely exhibits a Mg isotope heterogeneity as well. To assess the effects of secondary inclusions on Mg isotopes, several halite samples (IZ-2, DSDP546, Keuper-4, AW86-46, CAR12-3) were sampled from different locations within the salt specimen. Their Mg isotope values are homogeneous within ± 0.1‰, the external analytical precision (Table 2). Although not a total proof, the reproducibility of the Mg isotope results for halite at hand specimen scale is at least consistent with the idea that isotopic composition of Mg in halite can be accurately measured, which likely represents the Mg isotope signature of the brine from which the halite precipitated.

5.2. Isotopic variability of Mg in halite in geological history

The natural halite samples show significant variability in δ^{26}Mg values over the Phanerozoic (Fig. 6). First, we compare the Mg isotope data from halite with literature data for ancient seawater. Studies based on pelagic biogenic calcite sediments (Higgins and Schrag, 2015) and aragonite coral records (Gothmann et al., 2017) suggest that seawater δ^{26}Mg values over the Cenozoic varied little, around a modern value of −0.8‰. Calcite and aragonite records for Mg isotope compositions of seawater prior to 70 Ma are presently lacking, however, detailed studies of massive dolostones showed that δ^{26}Mg of seawater was −0.4‰ during the mid-Cretaceous (Li et al., 2019) and +0.3‰ during the early Triassic (Hu et al., 2017). The above Mg isotope data from various carbonate records are consistent with the modeled seawater δ^{26}Mg curve reported by Li et al. (2015). However, it is obvious that the majority of the halite samples that are older than 200 Ma are remarkably lower than the model curve of seawater δ^{26}Mg by Li et al. (2015), with the discrepancy well beyond the ± 0.1‰ level of the analytical uncertainty. For samples that are younger than 200 Ma, Mg isotope data from the halite are largely consistent with the modeled seawater curve.

We can further evaluate the halite Mg isotope data within the framework of global Mg cycling. Magnesium isotope composition of seawater is controlled by the balance between inputs of Mg into oceans via riverine runoffs, and removal of seawater Mg via dolomitization and hydrothermal alteration at mid-ocean ridges. During high-temperature hydrothermal alteration at mid-ocean ridges, Mg in seawater is quantitatively removed with little Mg isotope fractionation to be expected (Beinlich et al., 2014). Dolomite precipitation, by contrast, is accompanied by significant Mg isotope fractionation, with light Mg isotopes preferentially partitioned into dolomite (e.g., Fantle and Higgins, 2014; Higgins and Schrag, 2010; Li et al., 2015). As a result, seawater is expected to have δ^{26}Mg values higher than the δ^{26}Mg of average riverine input, and the offset between the two is positively correlated with the contribution of dolomitization to global Mg removal from seawater. The present-day global riverine runoff has a flux-weighted average δ^{26}Mg value of −1.09‰ (Tipper et al., 2006b). Assuming that δ^{26}Mg of global riverine input did not change significantly throughout the Phanerozoic, the seawater δ^{26}Mg would have been higher than −1.1‰, particularly for periods of Cambrian to Devonian, and the Triassic, when dolomitization intensity was high.

Additionally, we note that the δ^{26}Mg value of Miocene halite (DSDP134) from the Mediterranean Sea is higher than the well-constrained seawater value of −0.8‰ (Fig. 6). Considering that dolomitization was extensive in the Mediterranean during Miocene, it is not

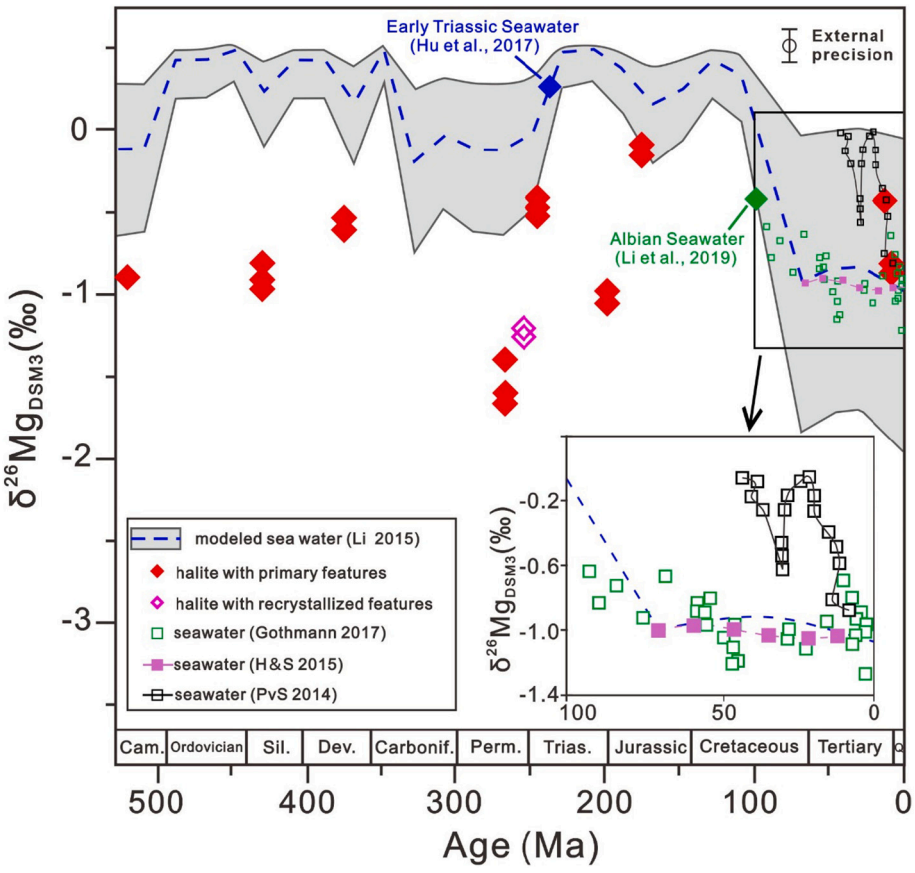

Fig. 6. Comparison of halite δ^{26}Mg values with the modeled seawater Mg isotope composition curve over the Phanerozoic. For comparison, the currently available magnesium isotope record of seawater is plotted (Gothmann et al., 2017; Higgins and Schrag, 2015; Hu et al., 2017; Li et al., 2019; Pogge von Strandmann et al., 2014). Pvs 2014—Pogge von Strandmann et al., 2014; H&S 2015—Higgins and Schrag, 2015; Li 2015—Li et al., 2015; Gothmann 2017—Gothmann et al., 2017.

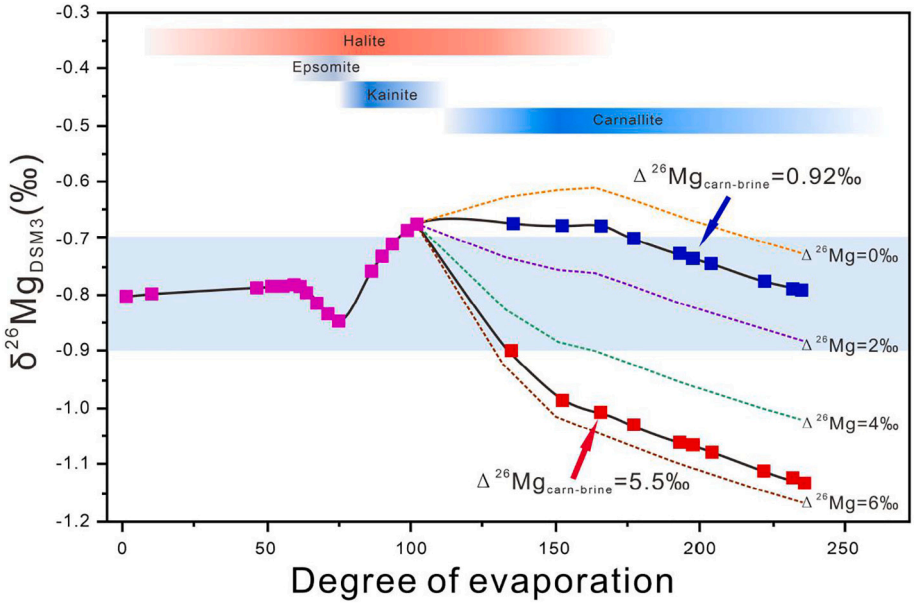

Fig. 7. The $\delta^{26}Mg$ evolution of brine with the degree of evaporation for modern seawater, based on data by Shalev et al. (2018b). The $\delta^{26}Mg$ value of the initial brine is set to −0.8‰ reported by Ling et al. (2011). The blue square and the red square respectively indicate different paths of the Mg isotope evolution of the brine due to the uncertainty of the fractionation factor between the carnallite and the aqueous solution. The isotope fractionation factors used for modeling of epsomite and kainite precipitation are based on literature data (Li et al., 2011; Li et al., 2015; Shalev et al., 2017; Wang et al., 2019). The fractional factor corresponding to the blue square is 0.92‰ and the red square corresponds to 5.50‰ (Shalev et al., 2017). (For interpretation of the references to color in this figure legend, the reader is referred to the web version of this article.)

surprising that the Mg isotope recorded by the Mediterranean Miocene halite sample (DSDP134) is heavier than the modeled coeval seawater Mg isotope value. To summarize, the halite Mg isotope record is variable and in many cases inconsistent with the literature data based on carbonate records or models.

5.3. Factors that affect the Mg isotope composition of halite record

The discrepancy between the Mg isotope data measured from the ancient halite deposits in this study and seawater Mg isotope data in the literature could be caused by the limitation of halite as a seawater Mg isotope archive. Indeed, ancient evaporite deposits have typically undergone complex geological processes, and certain syn- and post-depositional processes can cause Mg isotope compositions of some marine halite samples to deviate significantly from that of the modeled coeval seawater. Therefore, the possible processes and their isotopic effects are discussed below.

5.3.1. Evolution of brines due to mineral precipitation

As shown in Fig. 1, during the evaporation of seawater, precipitation of halite can take place for a long interval (DE ≈ 10–170, DE = degree of evaporation), and in the late stage of brine evaporation, Mg-containing minerals such as epsomite and carnallite start to precipitate (Bąbel and Schreiber, 2014; Shalev et al., 2018b). Meanwhile, due to Mg isotope fractionation between those minerals and aqueous solutions, the precipitation of Mg-bearing minerals would lead to the evolution of Mg isotopes in the brine. Halite precipitated from such evolved brines would record a different Mg isotope composition in its fluid inclusions.

In order to understand the isotopic effect of Mg-bearing evaporite minerals precipitation, we performed numerical modeling to quantitatively constrain the Mg isotope evolution of brine at different stages of evaporation. The core of the modeling is the isotope mass balance equation:

$$\delta^{26}Mg_{brine}(n) \times B(n) = \delta^{26}Mg_{brine}(n+1) \times B(n+1) + \delta^{26}Mg_{mineral}(n+1) \times M(n+1) \quad (1)$$

$\delta^{26}Mg_{brine}(n)$ denotes the Mg isotope composition of a brine that contains a Mg mass of B(n) at a given stage (n), and when this brine evolved to the next stage (n + 1), a Mg-bearing evaporite mineral is separated from the brine, removing Mg that has a mass of M(n + 1) and a Mg isotope composition of $\delta^{26}Mg_{mineral}(n+1)$, as a consequence, the Mg isotope composition of the brine evolves to $\delta^{26}Mg_{brine}(n+1)$, and the mass decreases to B(n + 1). Due to the conservation of mass of Mg, we have:

$$B(n) = B(n+1) + M(n+1) \quad (2)$$

Also, the Mg isotope fractionation between the brine and the precipitated can be described as:

$$\Delta^{26}Mg_{mineral-brine} = \delta^{26}Mg_{mineral}(n+1) - \delta^{26}Mg_{brine}(n+1) \quad (3)$$

The Mg isotope fractionation factor between epsomite and the $MgSO_4$-saturated solution ($\Delta^{26}Mg_{eps\text{-}sol}$) was experimentally calibrated to be 0.56‰ at T = 40 °C (Li et al., 2011). A 0.6‰ fractionation in $\delta^{26}Mg$ between the carnallite and the Dead Sea brine was reported (Gavrieli et al., 2009). However, a large range of fractionation for the same mineral ($\Delta^{26}Mg_{carnallite\text{-}brine}$ = +0.92 to +5.5‰) was later reported by (Shalev et al., 2017). The fractionation factors between other Mg-evaporites and brines have also been suggested (Shalev et al., 2017), such as $\Delta^{26}Mg_{bischofite\text{-}brine}$ = +0.33 ± 0.19‰, $\Delta^{26}Mg_{kainite\text{-}brine}$ = −1.3 ± 0.43‰, $\Delta^{26}Mg_{epsomite\text{-}brine}$ = +0.59 ± 0.31‰. Note that the Mg isotope fractionation factor between epsomite and the aqueous solution is consistent with the studies of Li et al. (2011) and Shalev et al. (2017).

In a recent study of Shalev et al. (2018b), detailed information about the mineralogy and mass of evaporite minerals in different precipitation stages of modern seawater have been reported. This study provides the information of B(n) and M(n) for a complete seawater evaporation sequence. Combining the $\Delta^{26}Mg_{mineral\text{-}brine}$, the B(n) and M(n), and Eqs. (1)–(3) mentioned above, we can construct a numerical model for the evolution of Mg isotope composition of brine in an evaporation sequence for seawater that has an initial $\delta^{26}Mg$ value of −0.8‰. The modeling results are shown in Fig. 7 and Supplement B, in which the $\delta^{26}Mg$ value of the brine is plotted against the degree of evaporation. Fig. 7 illustrates that fractional crystallization of epsomite and carnallite would decrease the $\delta^{26}Mg$ value of brine. For evaporation of modern seawater, the isotopic effect caused by epsomite precipitation is less significant due to the smaller Mg isotope fractionation factor and the narrower precipitation window for epsomite compared to carnallite. It should be noted there is large uncertainty in $\Delta^{26}Mg_{carnallite\text{-}brine}$ and further work is needed to better constrain such Mg isotope fractionation factor.

Additionally, it is important to note that because the seawater

chemistry varied significantly during the Phanerozoic (Horita et al., 2002; Lowenstein et al., 2001), the evaporation pathway of brines, including the mineralogy of evaporite minerals and their sequence and mass, may have been different in geological history. Nonetheless, a thick sequence of carnallite sandwiched between halite layers has been reported from evaporative basins (Cendon et al., 1998; Hardie, 1990). So, it is possible that the halite inclusions record isotopically evolved brines, which had δ^{26}Mg values lower than the initial seawater, although we note that deposition of carnallite generally requires a very high degree of evaporation and may not be common in evaporite records.

5.3.2. Entrapment of evaporite minerals into halite during syn-depositional process or post-depositional deformation

Co-precipitation of halite and Mg-bearing evaporite minerals (Lowenstein, 1988; Xu et al., 2016), as well as the tendency of halite beds to deform under specific stress and temperature conditions (Hudec and Jackson, 2007) lead to the possibility that the halite may entrapment other evaporite minerals during the syn-depositional process or post-depositional deformation. Salt diapirs are a common phenomenon and salt diapir structures with lengths and widths of a kilometer-scale have been widely reported from Germany, Iran, the Dead Sea and other regions (e.g., Al-Zoubi and ten Brink, 2001; Cheeney, 1992; Chemia et al., 2009; Strozyk et al., 2017). Salt deformation may induce mixing of the evaporites, resulting in entrapment of late-stage Mg-containing evaporite minerals into halite beds during the post-depositional deformation process. Post-depositional deformation of salt rocks might also lead to the migration of non-marine fluids along grain boundaries (Kukla et al., 2011) that potentially could affect the Mg isotope signature of the bulk halite.

Langbeinite ($K_2SO_4{\cdot}2MgSO_4$) and kainite are common evaporite salts that are enriched in light Mg isotopes (Feng et al., 2018; Shalev et al., 2017). If these minerals are entrapped with halite during the syn-depositional halite precipitation or post-depositional halite deformation, Mg isotope compositions of the bulk halite sample would be changed. The effect of evaporite mineral entrapment on bulk halite sample Mg isotope signature can be evaluated using a binary mixing model (Fig. 8). In the model we set that the brine trapped in fluid inclusions in halite has a δ^{26}Mg of −0.8‰, and the inclusions of evaporite minerals have Mg isotope compositions that are in equilibrium with the brine (i.e., $\delta^{26}Mg_{kain}$ = −2.1‰, $\delta^{26}Mg_{carn}$ = 0.12‰, $\delta^{26}Mg_{eps}$ = −0.24‰) based on reported Mg isotope fractionation factors (Li et al., 2011; Shalev et al., 2017). The δ^{26}Mg value of langbeinite ($\delta^{26}Mg_{lang}$ = −4.00‰) is measured from natural samples by Feng et al. (2018). The Mg isotope composition of the bulk halite is a function of the mineralogy of the mineral inclusion (Fig. 8), as well as the mass ratio of Mg in fluid inclusions and mineral inclusions. For example, to decrease the δ^{26}Mg of bulk halite by 0.5‰ relative to a mineral-inclusion-free halite sample, mineral inclusion could comprise of 15% of Mg in the halite for langbeinite, or 40% of Mg in the halite for kainite. If multiple Mg-bearing evaporite minerals are entrapped in the halite, then the Mg isotope composition of the dissolved bulk halite would additionally be controlled by the Mg mass ratio between the Mg-bearing minerals. The δ^{26}Mg values of Triassic polyhalite samples in the Sichuan Basin (around −1.00‰) are significantly lower than the modeled contemporaneous seawater (around 0.20‰, Li et al. (2015). Considering that Mg content in mineral inclusions could be significantly higher than that in fluid inclusions, entrapment of mineral inclusions (such as polyhalite) during syn-depositional co-precipitation and post-depositional deformation of halite could induce significant disturbance to the Mg isotope composition.

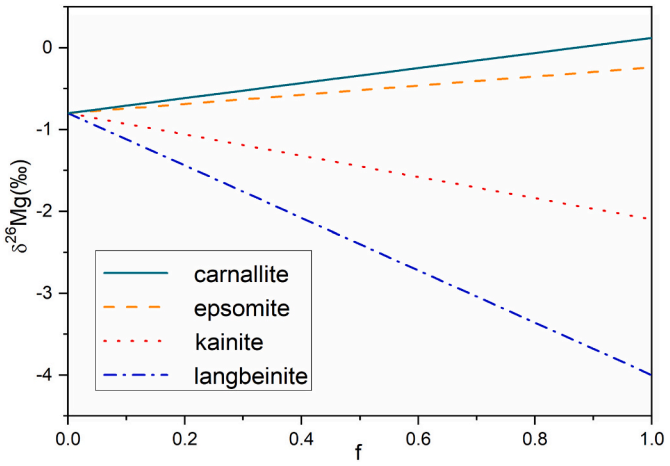

Fig. 8. The plot of δ^{26}Mg values of bulk halite sample versus the proportion of Mg from entrapped mineral inclusions. The δ^{26}Mg value of the initial brine is set to −0.8‰, f represents the proportion of Mg in entrapped mineral inclusions to bulk halite.

5.3.3. Recrystallization and dissolution of pre-existing Mg minerals

Recrystallization is well-known to affect Sr concentrations and isotopic compositions (Fantle and DePaolo, 2006; Richter and Liang, 1993), O isotope composition (Killingley, 1983; Schrag et al., 1995), Mg isotope composition (Chanda and Fantle, 2017; Fantle and Higgins, 2014) and Mg/Ca ratio of carbonates (Brown and Elderfield, 1996; Chanda et al., 2019). In this study, we also tested the effect of recrystallization on Mg isotopes in halite by analyzing the δ^{26}Mg values of five halite samples of similar ages from the Netherlands, which are characterized by distinct primary and recrystallized petrographic features. The results show that Mg in the recrystallized halite (Z2 & 7) is isotopically lighter (δ^{26}Mg = −1.24‰) than the pristine (recrystallization texture-free) halite (TWR-480 & 515), which have δ^{26}Mg of −0.44 to −0.50‰. Unless seawater δ^{26}Mg values can change by 0.8‰ within several million years, the results indicate that recrystallization can significantly affect the halite δ^{26}Mg value.

If recrystallization is the cause of the low δ^{26}Mg values of the Z2 & 7 halite, then the interstitial fluids in evaporites should contain isotopically light Mg. Based on the fact that carbonates are ubiquitous in sedimentary rocks and they generally have δ^{26}Mg values that are lower than −2‰, we hypothesize that the isotopically light Mg signatures in the halite sample could be originated from carbonate recrystallization during burial diagenesis. High-magnesium calcite (HMC) are known to be more soluble (thus less stable) than low-magnesium calcite (LMC) and aragonite (Andersson, 2005; Haese et al., 2014). Over time, HMC tends to transform into a more stable form of LMC during post-depositional processes, releasing Mg (Armenteros, 2010; Stanienda-Pilecki, 2018). The transformation process of HMC to LMC has been widely reported (e.g., Franchi et al., 2018; Frank and Lohmann, 1996; Sorauf and Webb, 2002; Zhuravlev and Wood, 2008). Because calcite precipitation is accompanied by large negative Δ^{26}Mg fractionation (Li et al., 2012; Mavromatis et al., 2012), the HMC to LMC transformation would be accompanied by the release of the light magnesium isotope into fluids in the sedimentary sequence, which could decrease the δ^{26}Mg of bulk halite if the halite is recrystallized in the fluid.

It should be noted that the δ^{26}Mg values of the recrystallized Zechstein halite samples from the Netherlands are higher than the halite samples from the largely coeval Salado Formation in New Mexico. Considering that catastrophic environmental changes occurred globally during the Permian-Triassic transition (e.g., Brand et al., 2012; Polozov et al., 2015; Sephton et al., 2015; Shen et al., 2011), a dramatic increase in seawater δ^{26}Mg value is a possibility that cannot be ruled out at the current stage. If so, a comparison of the Mg isotope compositions of halite from the two late Permian evaporite deposits would imply that halite recrystallization would increase in δ^{26}Mg value. If so, the Mg trapped by the recrystallized Zechstein halite from the Netherlands may not be related to HMC to LMC transformation.

Table 3
Comparison of the features of four seawater Mg isotope archives.

	Aragonite	Calcite	Dolomite	Halite
Direct record (no isotope fractionation)	No	No	No	Yes
Abundance in geological record	High	High	High	Medium
Robustness	Low	Medium	High	Medium to low
Easiness to diagnose resetting	High	Low	Low	Medium to low

5.4. Constraints on Mg isotope composition of ancient seawater: proxies versus models

At present, there are four types of geological archives available for seawater Mg isotopes, including three types of carbonates (aragonite, calcite, and dolomite) and one type of evaporite (halite) (Table 3). Among them, the carbonates are indirect recorders of seawater Mg isotope compositions as a specific isotope fractionation factor needs to be applied to the measured Mg isotope data from the carbonate. Although Mg isotope fractionation factors for the three carbonate minerals are available from experimental (e.g., Wang et al., 2013 for aragonite; Li et al., 2012 for calcite; Li et al., 2015 for dolomite) and theoretical studies (e.g., Pinilla et al., 2015; Rustad et al., 2010; Schauble, 2011), there are inconsistencies in fractionation factors for calcite between different experiments (e.g., Li et al., 2012 versus Mavromatis et al., 2013) and theoretical calculations (e.g., Pinilla et al., 2015; Rustad et al., 2010; Schauble, 2011). In addition, Mg isotope fractionation during carbonate precipitation could be affected by a number of factors such as precipitation rates, carbonate growth mechanism, or vital effects (e.g., Chen et al., 2020; Mavromatis et al., 2013). These issues add complexities to the attempts of using carbonates to reconstruct the Mg isotope composition of ancient seawater. From this perspective, the halite records have great advantages as seawater Mg isotope archive because they directly sampled ancient seawater/brine, and no correction of isotope fractionation factor is needed. Compared with carbonates, the occurrence of halite is less ubiquitous, nonetheless halite is still the most abundant phase in evaporite. Among the four seawater Mg isotope archives, dolomite has the highest robustness against post-depositional resetting due to its high Mg content and high thermodynamic stability (Hu et al., 2017). For comparison, halite is less robust as a recorder of seawater Mg isotopes, due to the low Mg content in halite and the tendency to deform under stress after burial. The greatest challenge to use halite as the ancient seawater recorder is probably the difficulty to diagnose resetting events from the sample. Very detailed petrographic observation is required for sample screening of halite. For comparison, aragonite has the greatest advantage as later alteration would result in the phase transition to the more stable calcite, which is easy to diagnose. To conclude, there is no perfect sedimentary archive for Mg isotopes in ancient seawater, but halite can complement the carbonate records due to its different features.

On the other hand, the Mg isotope composition of seawater in geological history could be calculated using models. Li et al. (2015) proposed a seawater δ^{26}Mg curve over the Phanerozoic based on a steady-state isotope mass balance equation, using the curve of the relative proportion of seawater Mg removal by marine dolomitization versus hydrothermal alteration at the mid-ocean ridge as compiled by Wikinson and Algeo (1989). The model curve successfully predicted relatively constant δ^{26}Mg values for seawater over the Cenozoic, as well as the higher δ^{26}Mg values of seawater during the early Triassic and the middle Cretaceous (Fig. 6), which had been confirmed by later studies using different carbonate records (Gothmann et al., 2017; Higgins and Schrag, 2015; Hu et al., 2017; Li et al., 2019). The inconsistency between the Mg isotope data from halite older than 200 Ma and the model curve of Li et al. (2015) therefore could reflect issues with the halite archive for Mg isotopes. However, it should be noted that the model of Li et al. (2015) has a number of limitations that could result in inaccurate seawater δ^{26}Mg values.

The first limitation is that Li et al. (2015) assumed a static global Mg isotope mass balance for seawater (i.e., Mg concentration and Mg isotope composition in steady-state at any given time), which is, although a reasonable simplification given the very long (> 10 Ma) residence time of Mg in modern seawater, not strictly correct as Mg content in seawater varied in geological times. The second limitation is that Li et al. (2015) assumed that the δ^{26}Mg value of global riverine runoff into the ocean remained a constant value of −1.09‰. It is a necessary assumption to construct a global Mg mass balance model. However, it is entirely possible that global riverine input had different δ^{26}Mg values in geological history due to the long-term evolution of tectonics and climates. The third limitation in the model of Li et al. (2015) is that the model relied principally on the Mg flux ratio data between dolomitization and high-temperature alteration at the mid-ocean ridge. However, more recent Mg isotope investigations on altered oceanic crusts (AOC), marine sediments, and low-temperature hydrothermal (LTH) fluids (Berg et al., 2019; Huang et al., 2018; Shalev et al., 2019) showed that low-temperature hydrothermal alteration at the mid-ocean ridge and silicate diagenesis also had a profound influence on the Mg isotope budget of ocean. Such effects were not considered in detail in the model of Li et al. (2015). Considering the above limitations, we should be cautious using the model curve of ancient seawater δ^{26}Mg values to evaluate the halite Mg isotope data. The inconsistency could also be caused by the inaccuracy of the model curve for ancient seawater δ^{26}Mg values. More work and tests are needed in the future to improve our understanding of secular seawater evolution in terms of its elemental and isotopic compositions.

6. Conclusions and outlooks

In this study, we developed a method to analyze the isotopic composition of Mg in halite. Using this method, we firstly measured Mg isotope compositions of a variety of Holocene and ancient halite samples. The marine halite samples show a large variation in δ^{26}Mg values, ranging from −0.1‰ to −1.6‰ relative to the DSM3 international Mg isotope standard. Our magnesium isotope data from some ancient salt samples are lighter than a modeled Mg isotope curve for seawater in literature. The possible reasons include: 1) evolution of brines due to mineral precipitation, 2) entrapment of evaporite minerals into halite during depositional or post-depositional deformation, 3) recrystallization and dissolution of pre-existing Mg minerals, 4) the limitations of modeling study for ancient seawater Mg isotope compositions.

This reconnaissance study of Mg isotope compositions of the marine halite deposits revealed the complexity of inclusions in ancient halite, and showed the importance of carefully characterizing the sedimentary background, stratigraphy, and petrology of evaporite for future Mg isotope studies of halite deposits. On the other hand, this study also implies that Mg isotopes in halite could provide unique information about syn-depositional and post-depositional processes the evaporites have experienced, even if they do not record uncontaminated contemporaneous seawater.

Supplementary data to this article can be found online at https://doi.org/10.1016/j.chemgeo.2020.119768.

Declaration of competing interest

The authors declare that they have no known competing financial interests or personal relationships that could have appeared to influence the work reported in this paper.

Acknowledgement

This manuscript benefits from constructive reviews from Xinyang Chen and three anonymous reviewers. We also thank Prof. Oleg Pokrovsky for his editorial handling and constructive comments. This work was supported by National Key R&D Program of China Project 2017YFC0602801 and National Natural Science Foundation of China (Grants No: 41622301, 41873004). This study was supported by ISF grant No. 2208/15 44890 to NDW and NSFC grant No. 41561144002 to WL, based on research agreements between the Israeli Science Foundation and the National Science Foundation of China.

References

Al-Zoubi, A., ten Brink, U.S., 2001. Salt diapirs in the Dead Sea basin and their relationship to Quaternary extensional tectonics. Mar. Pet. Geol. 18 (7), 779–797.
Andersson, A.J., 2005. Coastal Ocean and carbonate systems in the high CO2 world of the Anthropocene. Am. J. Sci. 305 (9), 875–918.
Armenteros, I., 2010. Chapter 2 diagenesis of carbonates in continental settings. In: Carbonates in Continental Settings: Geochemistry, Diagenesis and Applications. Developments in Sedimentology, pp. 61–151.
Arvidson, R.S., Guidry, M.W., Mackenzie, F.T., 2011. Dolomite controls on Phanerozoic seawater chemistry. Aquat. Geochem. 17 (4–5), 735–747.
Ayora, C., Fontarnau, R., 1990. X-ray microanalysis of frozen fluid inclusions. Chem. Geol. 89, 135–148.
Bąbel, M., Schreiber, B.C., 2014. Geochemistry of Evaporites and Evolution of Seawater. pp. 483–560.
Beinlich, A., Mavromatis, V., Austrheim, H., Oelkers, E.H., 2014. Inter-mineral Mg isotope fractionation during hydrothermal ultramafic rock alteration – implications for the global Mg-cycle. Earth Planet. Sci. Lett. 392, 166–176.
Belmaker, R., et al., 2013. 10Be dating of Neogene halite. Geochim. Cosmochim. Acta 122, 418–429.
Benison, K.C., 1995. Permian surface water temperatures from nippewalla group halite, Kansas. Carbonates Evaporites 10, 245–251.
Benison, K.C., Goldstein, R.H., Wopenka, B., Burrussk, R.C., Pasteris, J.D., 1998. Extremely acid Permian lakes and ground waters in North America. Nature 392, 911–914.
Berg, R., Solomon, E., Teng, F.-Z., 2019. The role of marine sediment diagenesis in the modern oceanic magnesium cycle. Nat. Commun. 10, 1–10.
Bialik, O.M., et al., 2018. Mg isotope response to dolomitization in hinterland-attached carbonate platforms: outlook of δ 26 Mg as a tracer of basin restriction and seawater Mg/Ca ratio. Geochim. Cosmochim. Acta 235, 189–207.
Biehl, B.C., Reuning, L., Strozyk, F., Kukla, P.A., 2014. Origin and deformation of intra-salt sulphate layers: an example from the Dutch Zechstein (Late Permian). Int. J. Earth Sci. 103 (3), 697–712.
Blättler, C.L., Miller, N.R., Higgins, J.A., 2015. Mg and Ca isotope signatures of authigenic dolomite in siliceous deep-sea sediments. Earth Planet. Sci. Lett. 419, 32–42.
Brand, U., et al., 2012. The end-Permian mass extinction: a rapid volcanic CO2 and CH4 -climatic catastrophe. Chem. Geol. 322-323, 121–144.
Brennan, S.T., Lowenstein, T.K., Cendon, D.I., 2013. The major-ion composition of Cenozoic seawater: the past 36 million years from fluid inclusions in marine halite. Am. J. Sci. 313 (8), 713–775.
Brown, S.J., Elderfield, H., 1996. Variations in Mg/Ca and Sr/Ca ratios of planktonic foraminifera caused by postdepositional dissolution: evidence of shallow Mg-dependent dissolution. Paleoceanography 11 (5), 543–551.
Cathro, D., Warren, J., Williams, G., 1992. Halite saltern in the Canning Basin, Western Australia: a sedimentological analysis of drill core from the Ordovician-Silurian Mallowa Salt. Sedimentology 39, 983–1002.
Cendon, D.I., Ayora, C., Pueyo, J.P., 1998. The origin of barren bodies in the Subiza potash deposit, Navarra, Spain: implications for sylvite formation. J. Sediment. Res. 68 (1), 43–52.
Chanda, P., Fantle, M.S., 2017. Quantifying the effect of diagenetic recrystallization on the Mg isotopic composition of marine carbonates. Geochim. Cosmochim. Acta 204, 219–239.
Chanda, P., Gorski, C.A., Oakes, R.L., Fantle, M.S., 2019. Low temperature stable mineral recrystallization of foraminiferal tests and implications for the fidelity of geochemical proxies. Earth Planet. Sci. Lett. 506, 428–440.
Cheeney, R.F., 1992. Salt Diapirs of the Great Kavir, Central Iran. Surv. Geophys. 13 (1), 89.
Chemia, Z., Schmeling, H., Koyi, H., 2009. The effect of the salt viscosity on future evolution of the Gorleben salt diapir, Germany. Tectonophysics 473 (3), 446–456.
Chen, X.-Y., et al., 2020. Experimental constraints on magnesium isotope fractionation during abiogenic calcite precipitation at room temperature. Geochim. Cosmochim. Acta 281, 102–117.
Clement, G., Holser, W.T., 1988. Geochemistry of Moroccan evaporites in the setting of the North Atlantic Rift. J. Afr. Earth Sci. (Middle East) 7, 375–383.
de Lange, G.J., Krijgsman, W., 2010. Messinian salinity crisis: a novel unifying shallow gypsum/deep dolomite formation mechanism. Mar. Geol. 275 (1), 273–277.
De Villiers, S., Dickson, J.A.D., Ellam, R.M., 2005. The composition of the continental river weathering flux deduced from seawater Mg isotopes. Chem. Geol. 216 (1–2), 133–142.
Dean, J.A., 1990. Lange's handbook of chemistry. Mater. Manuf. Process. 5 (4), 687–688.
Demicco, R.V., Lowenstein, T.K., Hardie, L.A., Spencer, R.J., 2005. Model of seawater composition for the Phanerozoic. Geology 33 (11), 877–880.
Du, D.-H., et al., 2017. Origin of heavy Fe isotope compositions in high-silica igneous rocks: a rhyolite perspective. Geochim. Cosmochim. Acta 218, 58–72.
Edmond, J.M., et al., 1979. Ridge crest hydrothermal activity and the balances of the major and minor elements in the ocean: the Galapagos data. Earth Planet. Sci. Lett. 46 (1), 1–18.
Elderfield, H., Schultz, A., 1996. Mid-ocean ridge hydrothermal fluxes and the chemical composition of the ocean. Annu. Rev. Earth Planet. Sci. 24 (1), 191–224.
Fanlo, I., Ayora, C., 1998. The evolution of the Lorraine evaporite basin: implications for the chemical and isotope composition of the Triassic ocean. Chem. Geol. 146, 135–154.
Fantle, M.S., DePaolo, D.J., 2006. Sr isotopes and pore fluid chemistry in carbonate sediment of the Ontong Java Plateau: calcite recrystallization rates and evidence for a rapid rise in seawater Mg over the last 10 million years. Geochim. Cosmochim. Acta 70 (15), 3883–3904.
Fantle, M.S., Higgins, J., 2014. The effects of diagenesis and dolomitization on Ca and Mg isotopes in marine platform carbonates: implications for the geochemical cycles of Ca and Mg. Geochim. Cosmochim. Acta 142, 458–481.
Feng, C.Q., Gao, C.H., Yin, Q.Z., et al., 2018. Tracking physicochemical conditions of evaporite deposition by stable magnesium isotopes: a case study of late Permian langbeinites. Geochem. Geophys. Geosyst. 19 (8), 2615–2630.
Franchi, F., et al., 2018. Petrographic and geochemical characterization of the early formative stages of Northern Adriatic shelf rocky buildups. Mar. Pet. Geol. 91, 321–337.
Frank, T.D., Lohmann, K.C., 1996. Diagenesis of fibrous magnesian calcite marine cement: implications for the interpretation of δ18O and δ13C values of ancient equivalents. Geochim. Cosmochim. Acta 60 (13), 2427–2436.
Fyfe, W.S., 1977. Effects on biological evolution of changes in ocean chemistry. Nature 267 (5611), 510.
Gavrieli, I., Yoffe, O., Burg, A., Halicz, L., 2009. Mg isotope fractionation in the Ca-chloride Dead Sea brine system. In: 19th Annual VM Goldschmidt Conference, pp. 220–224.
Geske, A., Goldstein, R.H., Mavromatis, V., et al., 2015. The magnesium isotope (δ26Mg) signature of dolomites. Geochim. Cosmochim. Acta 149, 131–151.
Gong, D., Hui, B., Zhou, J., 2018. Features of micro-fabric and the genetic study of Triassic deep polyhalite in the Guang'an area, central Sichuan Basin. China Geol. 1 (3), 453–454.
Gothmann, A.M., Stolarski, J., Adkins, J.F., Higgins, J.A., 2017. A Cenozoic record of seawater Mg isotopes in well-preserved fossil corals. Geology 45 (11), 1039–1042.
Haese, R.R., Smith, J., Weber, R., Trafford, J., 2014. High-magnesium calcite dissolution in tropical continental shelf sediments controlled by ocean acidification. Environ. Sci. Technol. 48 (15), 8522–8528.
Haq, B., Gorini, C., Baur, J., Moneron, J., Rubino, J.L., 2019. Deep Mediterranean's Messinian evaporite giant: how much salt? Glob. Planet. Chang. 184, 103052.
Hardie, L.A., 1990. The roles of rifting and hydrothermal CaCl2 brines in the origin of potash evaporites. Am. J. Sci. 290 (1), 43–106.
Hardie, L.A., 1996. Secular variation in seawater chemistry: an explanation for the coupled secular variation in the mineralogies of marine limestones and potash evaporites over the past 600 m.y. Geology 24 (3), 279–283.
Higgins, J.A., Schrag, D.P., 2010. Constraining magnesium cycling in marine sediments using magnesium isotopes. Geochim. Cosmochim. Acta 74 (17), 5039–5053.
Higgins, J.A., Schrag, D.P., 2015. The Mg isotopic composition of Cenozoic seawater – evidence for a link between Mg-clays, seawater Mg/Ca, and climate. Earth Planet. Sci. Lett. 416, 73–81.
Higgins, J., et al., 2018. Mineralogy, early marine diagenesis, and the chemistry of shallow-water carbonate sediments. Geochim. Cosmochim. Acta 220, 512–534.
Hinz, K., Winterer, E.L., 1984. Initial Reports of the Deep Sea Drilling Project, 79. Init. Rep. DSDP.
Holland, H.D., 2005. Sea level, sediments and the composition of seawater. Am. J. Sci. 305, 220–239.
Holser, W.T., Saltzman, E.S., Brookins, D.G., 1984. Geochemistry and petrology of evaporites cored from a deep-sea diapir at Site 546 offshore Morocco. Initial Rep. Deep Sea Drill. Proj. 79, 509–540.
Holt, N.M., García-Veigas, J., Lowenstein, T.K., Giles, P.S., Williams-Stroud, S., 2014. The major-ion composition of Carboniferous seawater. Geochim. Cosmochim. Acta 134, 317–334.
Horita, J., Matsuo, S., 1986. Extraction and isotopic analysis of fluid inclusions in halites. Geochem. J. 20, 261–272.
Horita, J., Friedman, T.J., Lazar, B., Holland, H.D., 1991. The composition of Permian seawater. Geochim. Cosmochim. Acta 55, 417–432.
Horita, J., Weinberg, A., Das, N., Holland, H.D., 1996. Brine inclusions in halite and the origin of the Middle Devonian Prairie Evaporites of Western Canada. Geochim. Cosmochim. Acta 66 (5), 956–964.
Horita, J., Zimmermann, H., Holland, H.D., 2002. Chemical evolution of seawater during the Phanerozoic: implications from the record of marine evaporites. Geochim. Cosmochim. Acta 66 (21), 3733–3756.

Hu, Z., et al., 2017. Resetting of Mg isotopes between calcite and dolomite during burial metamorphism: outlook of Mg isotopes as geothermometer and seawater proxy. Geochim. Cosmochim. Acta 208, 24–40.
Hu, Z., et al., 2019. Conservative behavior of Mg isotopes in massive dolostones: from diagenesis to hydrothermal reworking. Sediment. Geol. 381, 65–75.
Huang, K.J., Shen, B., Lang, X.G., et al., 2015. Magnesium isotopic compositions of the Mesoproterozoic dolostones: implications for Mg isotopic systematics of marine carbonates. Geochim. Cosmochim. Acta 164, 333–351.
Huang, K.J., Teng, F.Z., Plank, T., Staudigel, H., Hu, Y., Bao, Z.Y., 2018. Magnesium isotopic composition of altered oceanic crust and the global Mg cycle. Geochim. Cosmochim. Acta 238, 357–373.
Hudec, M.R., Jackson, M.P.A., 2007. Terra infirma: understanding salt tectonics. Earth Sci. Rev. 82 (1–2), 1–28.
Kampschulte, A., Buhl, D., Strauss, H., 1998. The sulfur and strontium isotopic compositions of Permian evaporites from the Zechstein basin, northern Germany. Geol. Rundsch. 87 (2), 192–199.
Killingley, J., 1983. Effects of diagenetic recrystallization on 18O/16O values of deep-sea sediments. Nature 301 (301), 594–597.
Knauth, L.P., Beeuna, M.A., 1986. Isotope geochemistry of fluid inclusions in Permian halite withimplications for the isotopic history of ocean water and the origin of saline formation waters. Geochim. Cosmochim. Acta 50 (3), 419–433.
Korte, C., Kozur, H., 2010. Carbon-isotope stratigraphy across the Permian–Triassic boundary: a review. J. Asian Earth Sci. 39, 215–235.
Kovalevych, V., Peryt, T.M., Beer, W., Geluk, M., Hałas, S., 2002. Geochemistry of Early Triassic seawater as indicated by study of the Röt halite in the Netherlands, Germany, and Poland. Chem. Geol. 182, 549–563.
Kukla, P.A., Reuning, L., Becker, S., Urai, J.L., Schoenherr, J., 2011. Distribution and mechanisms of overpressure generation and deflation in the late Neoproterozoic to early Cambrian South Oman Salt Basin. Geofluids 11 (4), 349–361.
Kushnir, J., 1982. The composition and origin of brines during the Messinian desiccation event in the Meditterranean Basin as deduced from concentrations of ions coprecipitated with gypsum and anhydrite. Chem. Geol. 35 (3), 333–350.
Lazar, B., Holland, H.D., 1988. The analysis of fluid inclusions in halite. Geochim. Cosmochim. Acta 59, 485–490.
Li, W., Beard, B.L., Johnson, C.M., 2011. Exchange and fractionation of Mg isotopes between epsomite and saturated MgSO4 solution. Geochim. Cosmochim. Acta 75 (7), 1814–1828.
Li, W., Chakraborty, S., Beard, B.L., Romanek, C.S., Johnson, C.M., 2012. Magnesium isotope fractionation during precipitation of inorganic calcite under laboratory conditions. Earth Planet. Sci. Lett. 333-334, 304–316.
Li, W., Beard, B.L., Li, C., Johnson, C.M., 2014. Magnesium isotope fractionation between brucite [Mg(OH)2] and Mg aqueous species: implications for silicate weathering and biogeochemical processes. Earth Planet. Sci. Lett. 394, 82–93.
Li, W., Beard, B.L., Li, C., Xu, H., Johnson, C.M., 2015. Experimental calibration of Mg isotope fractionation between dolomite and aqueous solution and its geological implications. Geochim. Cosmochim. Acta 157, 164–181.
Li, W., Beard, B.L., Li, S., 2016. Precise measurement of stable potassium isotope ratios using a single focusing collision cell multi-collector ICP-MS. J. Anal. At. Spectrom. 31 (4), 1023–1029.
Li, W., et al., 2019. Effects of early diagenesis on Mg isotopes in dolomite: the roles of Mn (IV)-reduction and recrystallization. Geochim. Cosmochim. Acta 250, 1–17.
Ling, M.X., et al., 2011. Homogeneous magnesium isotopic composition of seawater: an excellent geostandard for Mg isotope analysis. Rapid Commun. Mass Spectrom. 25 (19), 2828–2836.
Lowenstein, T.K., 1988. Origin of depositional cycles in the Permian “saline giant”: the Salado (McNutt zone) evaporites of New Mexico and Texas. Geol. Soc. Am. Bull. 100 (4), 592–608.
Lowenstein, T.K., Li, J., Brown, C.B., 1998. Paleotemperatures from fluid inclusions in halite: method verification and a 100,000 year paleotemperature record, Death Valley, CA. Chem. Geol. 150, 223–245.
Lowenstein, T.K., Timiifeeff, M.N., Brennan, S.T., Hardie, L.A., Demicco, R.V., 2001. Oscillations in Phanerozoic seawater chemistry: evidence from fluid inclusions. Science 294, 5544.
Lowenstein, T.K., Hardie, L.A., Timofeeff, M.N., Demicco, R.V., 2003. Secular variation in seawater chemistry and the origin of calcium chloride. Geology 31 (10), 857–860.
Lu, F., Meyers, W.J., 1998. Massive dolomitization of a late Miocene carbonate platform: a case of mixed evaporative brines with meteoric water, Nijar, Spain. Sedimentology 45, 263–277.
Lu, F.H., Meyers, W.J., Hanson, G.N., 2002. Trace elements and environmental significance of Messinian gypsum deposits, the Nijar Basin, southeastern Spain. Chem. Geol. 192 (3), 149–161.
Ma, H., et al., 2017. Heterogeneous Mg isotopic composition of the early Carboniferous limestone: implications for carbonate as a seawater archive. Acta Geochim. 37 (1), 1–18.
Mavromatis, V., et al., 2012. Magnesium isotope fractionation during hydrous magnesium carbonate precipitation with and without cyanobacteria. Geochim. Cosmochim. Acta 76, 161–174.
Mavromatis, V., Gautier, Q., Bosc, O., Schott, J., 2013. Kinetics of Mg partition and Mg stable isotope fractionation during its incorporation in calcite. Geochim. Cosmochim. Acta 114, 188–203.
McCaffrey, M.A., Lazar, B., Holland, H.D., 1987. The evaporation path of seawater and the coprecipitation of Br^- and K^+ with halite. J. Sediment. Petrol. 57 (5), 928–938.
Meilijson, A., Hilgen, F., Sepúlveda, J., et al., 2019. Chronology with a pinch of salt: integrated stratigraphy of Messinian evaporites in the deep Eastern Mediterranean reveals long-lasting halite deposition during Atlantic connectivity. Earth Sci. Rev. 194, 374–398.
Perez Fernandez, A., Berninger, U.N., Mavromatis, V., Pogge von Strandmann, P., Oelkers, E., 2017. Ca and Mg isotope fractionation during the stoichiometric dissolution of dolomite at temperatures from 51 to 126 °C and 5 bars CO 2 pressure. Chem. Geol. 467, 76–88.
Petrichenko, O.I., 1973. Methods of Study of Inclusions in Minerals of Saline Deposits (in Ukrainian: Translated in Fluid Inclusions Research COFFI, 12: 214–274, 1979). Naukova Dumka, Kiev.
Pinilla, C., Blanchard, M., Balan, E., Natarajan, S.K., Vuilleumier, R., Mauri, F., 2015. Equilibrium magnesium isotope fractionation between aqueous Mg2+ and carbonate minerals: insights from path integral molecular dynamics. Geochim. Cosmochim. Acta 163, 126–139.
Pogge von Strandmann, P.A.E., Forshaw, J., Schmidt, D.N., 2014. Modern and Cenozoic records of seawater magnesium from foraminiferal Mg isotopes. Biogeosciences 11 (18), 5155–5168.
Polozov, A.G., Svensen, H.H., Planke, S., Grishina, S., Fristad, K., Jerram, D.A., 2015. The basalt pipes of the Tunguska Basin (Siberia, Russia): high temperature processes and volatile degassing into the end-Permian atmosphere. Palaeogeogr. Palaeoclimatol. Palaeoecol. 441, 51–64.
Richter, F.M., Liang, Y., 1993. The rate and consequences of Sr diagenesis in deep-sea carbonates. Earth Planet. Sci. Lett. 117, 553–565.
Roberts, S.M., Spencer, R.J., 1995. Paleotemperatures preserved in fluid inclusions in halite. Geochim. Cosmochim. Acta 59 (19), 3929–3942.
Rustad, J., et al., 2010. Isotopic fractionation of Mg2+(aq), Ca2+(aq), and Fe2+(aq) with carbonate minerals. Geochim. Cosmochim. Acta 74, 6301–6323.
Ryan, W.B.F., Hsü, K.J., Cita, M.B., 1973. Boundary of Sardinia slope with Balearic Abyssal Plain at sites 133 and 134. Init. Rep. DSDP 13, 465–514.
Sandberg, P.A., 1983. An oscillating trend in Phanerozoic non-skeletal carbonate mineralgy. Nature 305, 19–22.
Schauble, E., 2011. First-principles estimates of equilibrium magnesium isotope fractionation in silicate, oxide, carbonate and hexaaquamagnesium(2+) crystals. Geochim. Cosmochim. Acta 75, 844–869.
Schrag, D.P., Depaolo, D.J., Richter, F.M., 1995. Reconstructing past sea surface temperatures: correcting for diagenesis of bulk marine carbonate. Geochim. Cosmochim. Acta 59 (11), 2265–2278.
Sephton, M., Jiao, D., Engel, M., Looy, C., Visscher, H., 2015. Terrestrial acidification during the end-Permian biosphere crisis? Geology 43, 159–162.
Shalev, N., Lazar, B., Halicz, L., Gavrieli, I., 2017. Mg isotope fractionation during precipitation of marine Mg-evaporites. In: Goldschmidt Abstract 2017.
Shalev, N., et al., 2018a. Mg isotope interlaboratory comparison of reference materials from earth-surface low-temperature environments. Geostand. Geoanal. Res. 42 (2), 205–221.
Shalev, N., Lazar, B., Köbberich, M., Halicz, L., Gavrieli, I., 2018b. The chemical evolution of brine and Mg-K-salts along the course of extreme evaporation of seawater – an experimental study. Geochim. Cosmochim. Acta 241, 164–179.
Shalev, N., Bontognali, T., Wheat, c., Vance, D., 2019. New isotope constraints on the Mg oceanic budget point to cryptic modern dolomite formation. Nat. Commun. 10, 5646.
Shannon, R.D., 1976. Revised effective ionic radii and systematic studies of interatomic distances in halides and chalcogenides. Acta Crystallogr. 751–767.
Shen, S., et al., 2011. Calibrating the end-Permian mass extinction. Science 334, 1367–1372.
Shepherd, T.J., Chenery, S.R., 1995. Laser ablation ICP-MS elemental analysis of individual fluid inclusions: an evaluation study. Geochim. Cosmochim. Acta 59 (19), 3997–4007.
Sirota, I., Arnon, A., Lensky, N.G., 2016. Seasonal variations of halite saturation in the Dead Sea. Water Resour. Res. 52 (9), 7151–7162.
Sorauf, J., Webb, G., 2002. Zigzag microstructure in rugose corals: a possible indicator of relative seawater Mg/Ca ratios. Geology 30 (5), 415–418.
Spear, N., et al., 2014. Analyses of fluid inclusions in Neoproterozoic marine halite provide oldest measurement of seawater chemistry. Geology 42 (2), 103–106.
Stanienda-Pilecki, K.J., 2018. Magnesium calcite in Muschelkalk limestones of the Polish part of the Germanic Basin. Carbonates Evaporites 33 (4), 801–821.
Stanley, S.M., Hardie, L.A., 1998. Secular oscillations in the carbonate mineralogy of reef-building and sediment-producing organisms driven by tectonically forced shifts in seawater chemistry. Palaeogeogr. Palaeoclimatol. Palaeoecol. 144, 3–19.
Stein, M., et al., 2000. The impact of brine-rock interaction during marine evaporite formation on the isotopic Sr record in the oceans: evidence from Mt. Sedom, Israel. Geochim. Cosmochim. Acta 64 (12), 2039–2053.
Strozyk, F., Reuning, L., Scheck-Wenderoth, M., Tanner, D.C., 2017. The Tectonic History of the Zechstein Basin in the Netherlands and Germany, Permo-Triassic Salt Provinces of Europe, North Africa and the Atlantic Margins. Elsevier, Amsterdam, Netherlands, pp. 221–241.
Sun, X.-H., et al., 2013. Composition determination of single fluid inclusions in salt minerals by laser ablation ICP-MS. Chin. J. Anal. Chem. 41 (2), 235–241.
Timofeeff, M.N., Lowenstein, T.K., Blackburn, W.H., 2000. ESEM-EDS: an improved technique for major element chemical analysis of fluid inclusions. Chem. Geol. 164, 171–182.
Tipper, E., Galy, A., Bickle, M., 2006a. Riverine evidence for a fractionated reservoir of Ca and Mg on the continents: implications for the oceanic Ca cycle. Earth Planet. Sci. Lett. 247 (3–4), 267–279.
Tipper, E., et al., 2006b. The magnesium isotope budget of the modern ocean: constraints from riverine magnesium isotope ratios. Earth Planet. Sci. Lett. 250 (1–2), 241–253.
Veizer, J., et al., 1997. Oxygen isotope evolution of Phanerozoic seawater. Palaeogeogr. Palaeoclimatol. Palaeoecol. 132, 159–172.
Veizer, J., et al., 1999. 87Sr/86Sr, δ13C and δ18O evolution of Phanerozoic seawater. Chem. Geol. 161 (1), 59–88.
Vengosh, A., Starinsky, A., Anati, D.A., 1994. The origin of Mediterranean interstitial

water—— relics of ancient Miocene brines: a re-evaluation. Earth Planet. Sci. Lett. 121, 613–627.
von Borstel, L.E., Zimmermann, H., Ruppert, H., 2000. Fluid inclusion studies in modern halite from the Inagua solar saltwork. In: 8th World Salt Symposium. vol.2 Elsevier Science, Amsterdam (673-678 pp).
Wang, S.L., Zheng, M.P., 2014. Discovery of Triassic polyhalite in Changshou area of East Sichuan Basin and its genetic study. Mineral Deposits 33, 1045–1056 (in Chinese with English abstract).
Wang, Z., et al., 2013. Experimental calibration of Mg isotope fractionation between aragonite and seawater. Geochim. Cosmochim. Acta 102, 113–123.
Wang, W., Zhou, C., Liu, Y., Wu, Z., Huang, F., 2019. Equilibrium Mg isotope fractionation among aqueous Mg2+, carbonates, brucite and lizardite: insights from first-principles molecular dynamics simulations. Geochim. Cosmochim. Acta 250, 117–129.
Warren, J.K., 2006. Evaporites: Sediments, Resources and Hydrocarbons.
Wikinson, B.H., Algeo, T.J., 1989. Sedimentary carbonate record of calcium-magnesium cycling. Am. J. Sci. 289, 1158–1194.
Wimpenny, J., Colla, C.A., Yin, Q.-Z., Rustad, J.R., Casey, W.H., 2014. Investigating the behaviour of Mg isotopes during the formation of clay minerals. Geochim. Cosmochim. Acta 128, 178–194.
Wombacher, F., et al., 2011. Magnesium stable isotope fractionation in marine biogenic calcite and aragonite. Geochim. Cosmochim. Acta 75 (19), 5797–5818.
Xu, H., Guo, X., Bai, J., 2016. Thermal behavior of polyhalite: a high-temperature synchrotron XRD study. Phys. Chem. Miner. 44 (2), 125–135.
Zak, I., 1967. The Geology of Mount Sdom. Hebrew University, Jerusalem (208 pp).
Zak, I., 1997. Evolution of the Dead Sea brines. In: The Dead Sea: The Lake and Its Setting. Oxford University Press.
Zambito, J.J., Benison, K.C., 2013. Extremely high temperatures and paleoclimate trends recorded in Permian ephemeral lake halite. Geology 41 (5), 587–590.
Zhong, J., et al., 2018. Sedimentary characteristics and genetic study of deep polyhalite in Huangjingkou anticline of northeast Sichuan. Mineal Depos. 37, 81–90 (in Chinese with English abstract).
Zhuravlev, A.Y., Wood, R.A., 2008. Eve of biomineralization: controls on skeletal mineralogy. Geology 36 (12), 923–926.